Phenotypic Discovery of Triazolo[1,5-*c*]quinazolines as a First-In-Class Bone Morphogenetic Protein Amplifier Chemotype

Fabian Wesseler, Stefan Lohmann, Daniel Riege, Jonas Halver, Aileen Roth, Christian Pichlo, Sabrina Weber, Masanari Takamiya, Eva Müller, Jana Ketzel, Jana Flegel, Adrian Gihring, Sepand Rastegar, Jessica Bertrand, Ulrich Baumann, Uwe Knippschild, Christian Peifer, Sonja Sievers, Herbert Waldmann, and Dennis Schade*

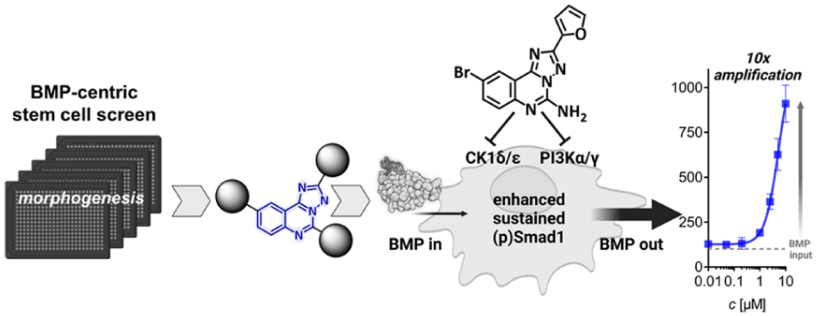

ABSTRACT: Phenotypic drug discovery (PDD) continues to fuel the research and development pipelines with first-in-class therapeutic modalities, but success rates critically depend on the quality of the underlying model system. Here, we employed a stem cell-based approach for the target-agnostic, yet pathway-centric discovery of small-molecule cytokine signaling activators to act as morphogens during development and regeneration. Unbiased screening identified triazolo[1,5-*c*]quinazolines as a new-in-class in vitro and in vivo active amplifier of the bone morphogenetic protein (BMP) pathway. Cellular BMP outputs were stimulated via enhanced and sustained availability of BMP-Smad proteins, strictly dependent on a minimal BMP input. Holistic target deconvolution unveiled a unique mechanism of dual targeting of casein kinase 1 and phosphatidyl inositol 3-kinase isoforms as key effectors for efficient amplification of osteogenic BMP signaling. This work underscores the asset of PDD to discover unrecognized polypharmacology signatures, in this case significantly expanding the chemical and druggable space of BMP modulators.

1. INTRODUCTION

Organ development and regeneration is largely governed by the action of growth factors/cytokines. In this regard, genuine small-molecule activators of cytokine signaling are highly attractive therapeutic modalities for several disease states, particularly within the field of regenerative medicine. However, their rational development remains inherently challenging and mostly relies on profound knowledge of the underlying pathway biology to fuel target-centric drug discovery (TDD) campaigns. Only few marketed examples exist, including the thrombopoietin mimetics Eltrombopag and Lusotrombopag or Bayers' recently approved Molidustat, which does not act as a direct activator but stimulates the expression of erythropoietin by targeting hypoxia-inducible factor prolyl hydroxylase.[1−3]

We envisioned that employment of relevant cellular systems might enable the discovery of new small-molecule cytokine signaling activators. More specifically, for tissue regeneration, capturing cytokine functions as morphogens rather than assessing their plain effects on single-cell fates might be critical to expand the druggable space of small-molecule regenerative agents. To do this, meaningful phenotypic assays in a developmental context are required. We have recently exemplified the feasibility of such a pathway-focused yet target-agnostic screening platform for the discovery of bone morphogenetic protein (BMP) signaling activators.[4] BMPs belong to the transforming growth factor-β (TGFβ) family of ligands and largely gained attention for their osteoinductive potential to treat skeletal trauma and osteopenic diseases.[5−7] We showed that the role of BMP could be functionally probed during cardiogenic mesoderm patterning from embryonic stem cells in a quite selective and high-throughput-compatible fashion. A proof-of-concept chemical screen afforded 2,3-

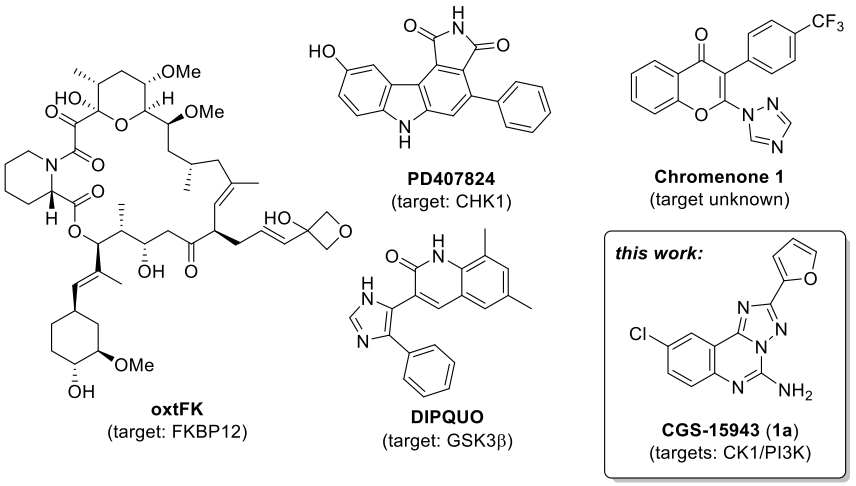

Figure 1. Chemical structures of BMP signaling activator modalities. The tacrolimus (FK506)-derived oxtFK targets the FK506 binding protein 12 (FKBP12),[11] which serves as an endogenous repressor of BMP receptor type I activity. DIPQUO acts as a glycogen synthase kinase 3-β (GSK3β) inhibitor,[10] and PD407824 was reported to enhance BMP via checkpoint kinase 1 (CHK1) inhibition, resulting in a p21-cyclin-dependent kinase 9 (CDK9)-dependent downregulation of TGFβ-Smads.[9] Chromenone 1 also potentiates canonical BMP outputs at the expense of TGFβ-Smads, but without affecting kinase-driven cascades.[4] This work discloses triazolo[1,5-*c*]quinazoline CGS-15943 (**1a**), which targets specific casein kinase 1 (CK1) and phosphatidyl inositol-3 kinase (PI3K) isoforms for BMP pathway amplification.

disubstituted 4*H*-chromen-4-ones (Figure 1) as a novel and mechanistically interesting class of BMP potentiators with osteogenic efficacy.[4]

Although Chromenone 1 already displayed several advantageous features compared to the few reported well-characterized BMP potentiators, including Ventromorphin,[8] PD-407824,[9] DIPQUO,[10] and oxtFK (Figure 1),[11] its mode of action involved the downregulation of TGFβ-Smads. For therapeutic applications, however, it would be desirable to boost signaling outputs in a strongly BMP-dependent and -exclusive fashion without excessive perturbation of closely related developmental pathways. Herein, we report the discovery of a class of triazolo[1,5-*c*]quinazolines that fulfill these criteria. This chemotype was identified with CGS-15943 (**1a**, Figure 1) from our stem cell-based phenotypic drug discovery deck. **1a** functions as an in vitro- and in vivo-active, osteogenic BMP signaling amplifier with a unique mechanistic profile, which involves the inhibition of specific casein kinase 1 (CK1) and phosphatidyl inositol-3 kinase (PI3K) isoforms.

2. RESULTS AND DISCUSSION

2.1. Discovery and Validation of Triazolo[1,5-*c*]-quinazoline 1a as a Novel BMP Amplifier Chemotype.

BMPs play multiple roles during embryonic development. For instance, they are essential in early dorsoventral patterning of mesoderm and in the morphogenesis of several organs.[5,12] Building on this knowledge, we recently devised a phenotypic drug discovery (PDD) assay that functionally recapitulates BMP signaling during cardiogenic mesoderm patterning from murine embryonic stem cells (mESCs).[4] In brief, mESCs that stably express a cardiac marker (i.e., *Myh6*-GFP) are stimulated with the selective BMP inhibitor DMH-1 during a highly BMP-specific time frame of cardiogenic mesoderm formation. DMH-1-induced cardiogenesis can then be antagonized by co-treatment with BMPs or a BMP-mimicking small molecule, respectively. High-content imaging analysis robustly quantifies GFP$^+$ cardiomyocyte clusters as the ultimate phenotypic readout downstream of differentiation. BMP-mimicking or -activating small molecules are followed up as hits when *Myh6*-GFP levels are reduced <30% compared to DMSO without affecting total cell numbers (DAPI$^+$ nuclei count). Unbiased screening of the LOPAC/Prestwick library of pharmacologically active compounds in this BMP-focused morphogenic mESC assay furnished 12 IC_{50}-validated hits (i.e., 0.71% hit rate) that were further filtered for potency on a BMP-response element reporter (BRE-*Vent2*),[4,13,14] followed by selectivity profiling against the closely related TGFβ, Activin/Nodal (SBE4 reporter), and Wnt/β-Catenin (TCF reporter) pathways (Figures 2 and S1). Following this hit selection logic, triazolo[1,5-*c*]quinazoline **1a** emerged as a prime hit candidate with submicromolar activity in the mESC assay (IC_{50} = 0.5 μM) that functionally mimicked BMP as further confirmed by expression analysis of the key BMP target gene *Id1* in this setup (Figure 2B).[4,15,16] **1a** exhibited a superior profile among all validated hits based on its potent activation of a BRE reporter (280 ± 68%, Figure 2C) as well as selectivity against TGFβ/ActA, Sonic Hedgehog (GLI reporter),[17] and Wnt/βCatenin (Figures 2D and S1).

In view of our ultimate aim to develop BMP stimulators with osteoinductive efficacy for pharmacological bone regeneration, an orthogonal BMP-dependent assay was employed to assess the compounds' functionality on osteoblastogenesis. Indeed, **1a** potently stimulated osteogenic differentiation in C2C12 cells (256 ± 36%, Figure 2E). The osteogenic phenotype was not just evaluated by activity and expression of alkaline phosphatase (*Alp*). BMP-dependent, osteogenic transcription (*Runx2*, runt-related transcription factor 2) and early (*Ocn*, osteocalcin) as well as late osteoblast markers (*Osx*, osterix) were additionally quantified and confirmed BMP-driven osteoblast formation (Figure 2F). Moreover, **1a** stimulated osteoblast differentiation and maturation in a human cell context (i.e., SaOS-2 cells) in synergy with BMP-2 and BMP-4 (Figure 2G). Although the effect was only significant for BMP-2, the same trend was observed for BMP-4.

Notably, **1a** mimicked the action of BMP in the original morphogenic stem cell assay, while reporter gene assays in HEK293T cells and osteogenic differentiation in C2C12 cells required addition of BMP ligand. A minimal BMP-4 dose of

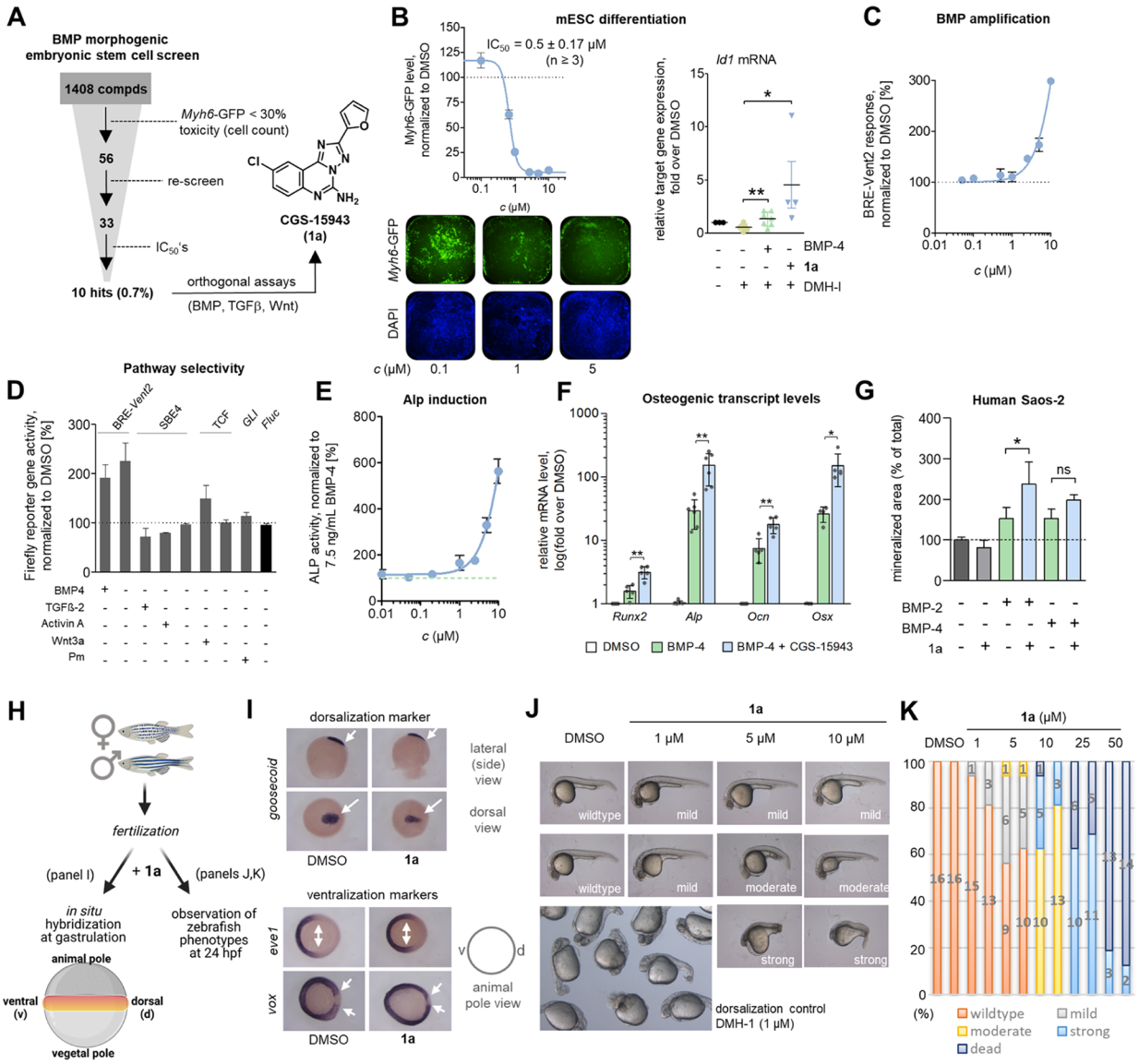

Figure 2. Phenotypic stem cell screen identifies triazolo[1,5-*c*]quinazoline **1a** as a potent, selective, and osteogenic BMP signaling amplifier with in vitro and in vivo efficacies. (A) Screening and validation workflow to identify CGS-15943 (1a) as a prime hit: 1° image-based screening in mESCs with 30% *Myh6*-GFP level cutoff and toxicity (cell count) for hit selection, IC_{50}-validation of confirmed hits, and 2° screening in 293T cells for pathway selectivity (reporter gene assays). (B) Dose−response profile of 1a displays high potency and efficacy as BMP-4-mimetic during mESC cardiogenesis; data shown as means ± SEM ($n \geq 3$); representative images of 1a-treated mESCs after fixation showing cardiac *Myh6*-GFP levels and total cells (DAPI); functional confirmation of 1a (2.5 μM) with BMP mimetic efficacy during mESC cardiogenesis (24 h between d3-4 of differentiation) by relative quantification of *Id1* gene expression; data are shown as mean ± SEM ($n \geq 4$, normalized to DMSO); statistical analysis was performed by unpaired *t*-tests (*$p < 0.05$; **$p < 0.01$). (**C**) **1a** potently amplifies BMP-4 (10 ng/mL) signaling in a BMP-response element luciferase reporter (BRE-*Vent2*) assay in HEK293T cells; data are shown as mean ± SD activity ($n \geq 6$) and normalized to DMSO vehicle (= 100%). (D) Reporter gene assay profiling in HEK293T cells reveals a high selectivity of **1a** (5 μM) for BMP (BRE-*Vent2*) versus TGFβ/Activin A (SBE4), Wnt (TCF), and sonic hedgehog (GLI); pathways were activated with the respective growth factors at 10 ng/mL or purmorphamine (1.5 μM, *Pm*) for sonic hedgehog (Shh) activation; data are shown as mean ± SD ($n \geq 3$) and normalized to DMSO vehicle (= 100%). (E) Dose−response profile of **1a** on C2C12 osteoblast differentiation (% ALP activity) compared to low-dosed BMP-4 (7.5 ng/mL); data are shown as mean ± SD ($n \geq 6$), normalized to 7.5 ng/mL BMP-4 (= 100%). (F) Relative quantification of BMP-dependent osteogenic gene expression transcripts confirmed **1a** as an authentic BMP amplifier; C2C12 cells were treated with BMP-4 (7.5 ng/mL) and **1a** (5 μM) or DMSO (vehicle control) for 72 h; data are shown as mean ± SD ($n \geq 3$), normalized to DMSO; statistical analysis was performed by unpaired two-tailed *t*-test (*$p < 0.05$; **$p < 0.01$; ***$p < 0.001$). (G) Osteoblastic mineralization in the human osteosarcoma cell line (SaOS-2) was induced by **1a** after 11 days of osteogenic differentiation: Alizarin Red staining was used for image-based quantification of mineralization; data shown as mean ± SEM ($n \geq 3$); statistical analysis was performed using one-way ANOVA test (*$p < 0.05$). (H−K) In vivo efficacy of **1a** as a BMP signaling activator during zebrafish embryo development was assessed by whole mount in situ hybridization during gastrulation and by analysis of the embryo phenotypes at 24 hpf: (I) note a reduction in the expression of *goosecoid* in most dorsal (= d) mesoderm and an increase of ventral (= v) markers *eve1* and *vox* exposed to 2 μM of **1a** (right panels) or DMSO vehicle (left panels); (J) representative images of dose-dependent (1−10 μM) induction of ventralized phenotypes by **1a** at 24 hpf, DMH-1 (1 μM)-induced dorsalized phenotypes are depicted as controls; (K) quantitative distribution of embryo phenotypes at different concentrations of **1a** (1−50 μM) for at least 15 embryos per condition.

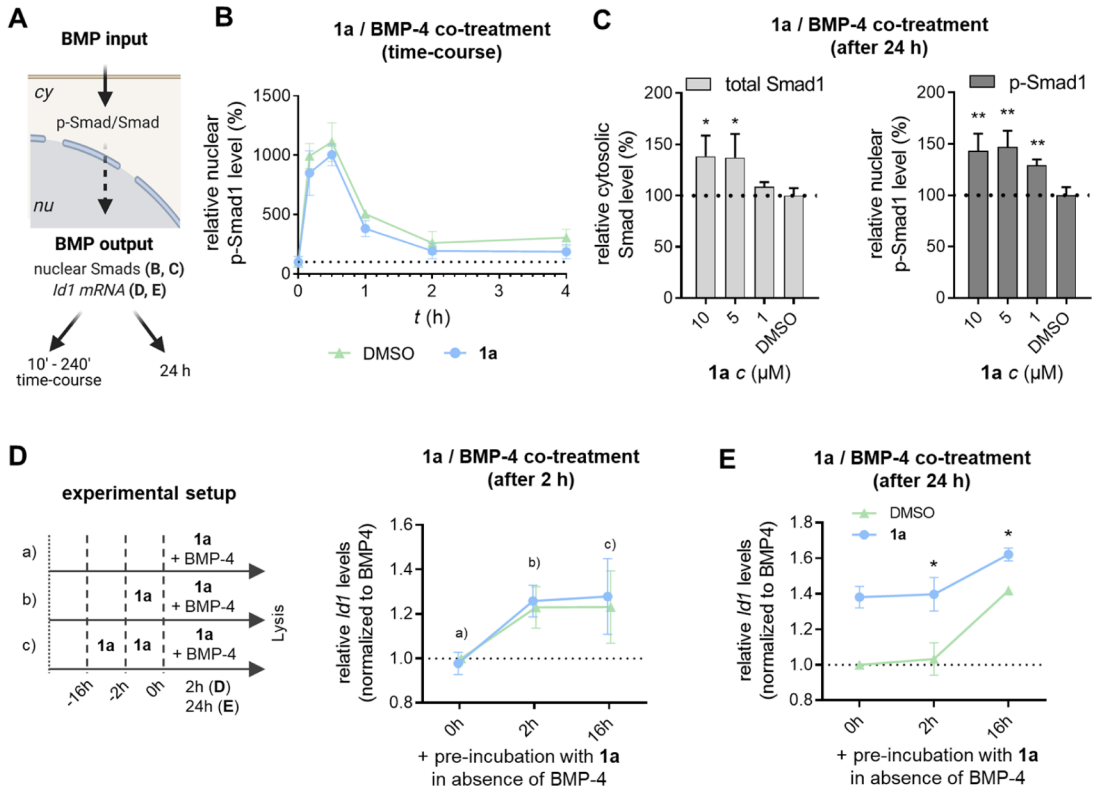

Figure 3. BMP signaling dynamics reveal BMP input-dependent enhancement of Smad1 by **1a**. (A) Schematic illustration of the experimental setups to analyze BMP signaling dynamics during C2C12 osteoblastic differentiation. (B) Time course of nuclear phospho-Smad1 levels shows rapid accumulation of nuclear *p*-Smad1 in response to BMP-4, which remained unchanged upon co-treatment with **1a**. DMSO vehicle, 7.5 ng/mL BMP-4, or **1a** (5 μM) was incubated for 240 min, and lysates were collected on indicated time points, followed by subcellular fractionation and Western blotting. Data are shown as mean ± SD (n = 3) and normalized to t_0. (C) Co-treatment of BMP-4 and **1a** leads to increased cytosolic Smad1 levels after 24 h, thereby increasing responsiveness toward subsequent BMP input, resulting in higher nuclear phospho-Smad1 levels. C2C12 were treated with 7.5 ng/mL BMP-4 and 1a. Data are shown as mean ± SD (n = 3), statistical significance calculated by unpaired t-test, *p < 0.05; **p < 0.01. (D,E) Relative quantification of BMP-dependent *Id1* expression (qPCR) upon co-treatment of BMP-4 and **1a** reveals *Id1* upregulation after 24 h but not after 2 h, not even when pre-incubated with **1a** in the presence of BMP-4. Co-treatment of BMP-4 (7.5 ng/mL, green) and **1a** (5 μM, blue) was performed for 2 h (**C**) or 24 h (**D**) with **1a** pre-incubated for 0 h, 2 h, and 16 h. Data points represent mean ± SD, normalized to 7.5 ng/mL BMP-4. Statistical analysis was performed with an unpaired two-tailed t-test (*p < 0.05).

only 10 pg/mL suffices for a highly efficient signaling amplification by **1a** (up to 4-fold) in HEK cells (Figure S1D), and at least 2.5−5 ng/mL was required in C2C12 cells to enhance osteoblastogenesis (up to 6-fold, Figure S1E). This observation is intriguing as it points at the peculiarity of morphogenic cytokine signaling for tissue/organ development and regeneration from stem/progenitor cells. Hence, we asked whether this is also the case under in vivo conditions. Indeed, **1a** effectively boosted BMP signaling in developing zebrafish embryos without exogenously complementing BMP. In these experiments, when zebrafish embryos were exposed to 2 μM of **1a** at 3 h post fertilization (hpf), they showed a typical ventralized phenotype characteristic of BMP overexpression (Figure 2H−K).[18] In agreement with the observed ventralized phenotype, the treated embryos, assayed by whole mount in situ hybridization, also showed an expansion of ventral mesoderm markers such as *even-skipped-like 1* (*eve1*) and *ventral homeobox* (*vox*) into the dorsal mesoderm at the expense of the dorsal marker gene *goosecoid* (*gsc*). Interestingly, the number of ventralized embryos was increased upon **1a** treatment with higher concentrations up to 10 μM. A batch of embryos exposed to greater doses than 10 μM showed an important increase in mortality, suggestive of toxic effects on embryo development.

Collectively, triazolo[1,5-*c*]quinazoline **1a** efficiently amplifies BMP signaling where it plays decisive physiological roles, demonstrated here in the context of osteoblast formation, mesodermal patterning from embryonic stem cells in vitro, and in analogy, dorso-ventral structuring during gastrulation in vivo.

2.2. CGS-15943 (1a) Amplifies BMP Outputs by Enhanced and Sustained Smad1 Availability. BMP signaling is initiated by heterodimerization of the type I and constitutively active type II receptors upon binding of dimeric ligands, inducing *trans*-phosphorylation of the type I receptor that subsequently activates cytosolic R-Smads (i.e., Smads 1, 5, 8/9).[19,20] R-Smads form a complex with a Co-Smad (i.e., Smad4), which translocates to the nucleus and regulates the expression of BMP target genes, including the *inhibitor of DNA binding* (*Id*) gene family.[21] Intriguingly, we found that activation of BMP signaling by **1a** seemed to require only minimal ligand input that is typically provided during tissue/organ development in a spatio-temporal manner, thus functioning as an amplifier of actual morphogenic signaling. Therefore, we next characterized whether and how this action is mediated by canonical downstream events on a time scale. To do this, the dynamics of Smad1 phosphorylation and

Scheme 1. Synthetic Routes to Access Diversely Substituted triazolo[1,5-*c*]quinazolines and Related Scaffold Derivatives[a]

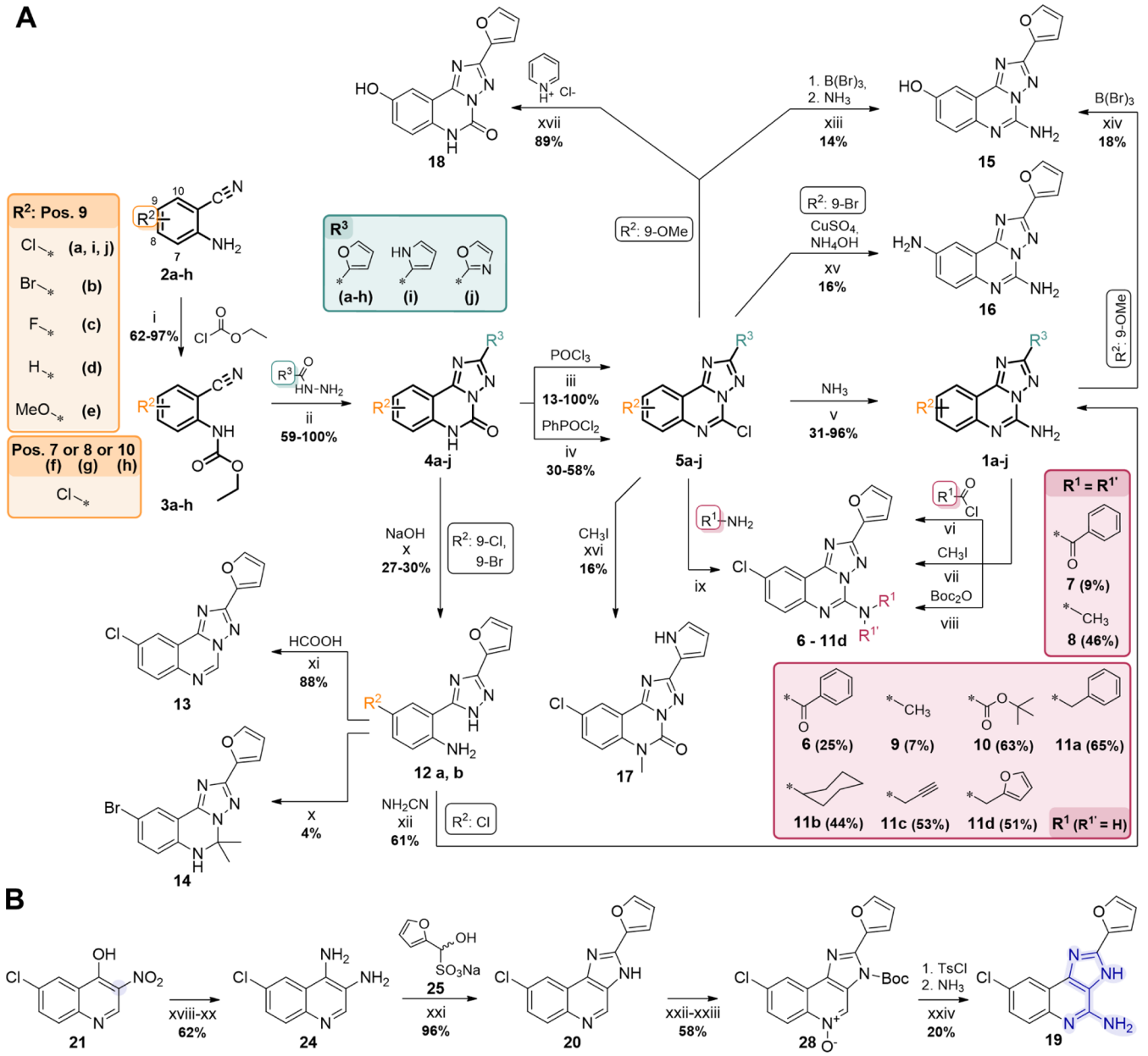

[a](A) (i) reflux, 3−13 h; (ii) carbohydrazide, NMP, 160 °C, 6−18 h; (iii) DIPEA, reflux, 22−42 h (**4a**, **d**−**j**); (iv) 185 °C, 20−22 h (**4b** + **c**); (v) NH_3 (7M in MeOH), THF, ambient, 3−23 h; (vi) benzoyl chloride, DIPEA, microwave, 125 °C, 1 h, 25% (**6**), 9% (**7**); (vii) NaH, TBAB, THF, ambient, 4 h, 46% (**8**), 7% (**9**); (viii) DMAP, THF, reflux, 1 h; (ix) amine, microwave, 80−140 °C, 15 min, 44−65%; (x) ethylene glycol, 135 °C, 17−35 h, 27% (**12b**), 30% (**12a**); (xi) reflux, 10 h; (xii) NH_2CN (50% aqueous), H_2SO_4, *i*-Pr, reflux, 9 h; (xiii) 1.: $B(Br)_3$, DCM, ambient, 96 h; 2.: NH_3 (7M in MeOH), THF, 50 °C, 24 h; (xiv) $B(Br)_3$, DCM, 96 h; (xv) NH_4OH (conc), $CuSO_4 \cdot 5\ H_2O$, 140 °C, 154 h; (xvi) NaH, THF, ambient, 22 h; (xvii) 170 °C, 4.5 h. (B) (xviii) $SOCl_2$, DMF (cat), DCM (neat), reflux, 6 h, 85%; (xix) NH_3 (7M in MeOH), THF (neat), 0 °C → ambient, 3 h, 93%; (xx) $Na_2S_2O_4$, EtOH/H_2O, reflux, 1 h, 79%; (xxi) DMF, 100 °C, 4.5 h; (xxii) Boc_2O, DMAP, N_2, THF (neat), reflux, 4 h, 79%; (xxiii) *m*-CPBA, DCM, ambient, 3−3.5 h, 74%; (xxiv) 1. Ar, $PhCF_3$/DCM (neat), 0 °C, 4 h, 2. NH_3 (7M in MeOH), ambient, overnight.

localization were characterized during C2C12 osteoblast differentiation as outlined in Figure 3A.

Nuclear phosphorylated Smad1 levels were quantified over the course of 240 min. Upon BMP stimulus, instant phosphorylation events were not affected by **1a** (Figure 3B). However, after 24 h of co-treatment with BMP-4, both nuclear phospho-Smad1 and total Smad1 protein levels were increased in a dose-dependent fashion (Figure 3C). To substantiate these findings, the expression of *Id1* as the key canonical target gene was followed over time along with other direct (*Id2,-3*) or indirect BMP target genes (*Runx2, Osx*) (Figures 3D,E and S3A,B). Again, after short co-treatment of **1a**/BMP-4 (2 h), no increased signaling outputs were detected (Figure 3C). Importantly, this was also not the case when cells were incubated for 2 or 16 h with **1a** *prior* to the actual BMP-4 stimulus (= pre-treatment). This intriguing result suggested that cells cannot even be "primed" for BMP amplification by **1a** in the complete absence of basal signaling activation. However, when co-treatment with **1a**/BMP-4 was prolonged from 2 to 24 h, *Id1* expression was significantly enhanced. Once more,

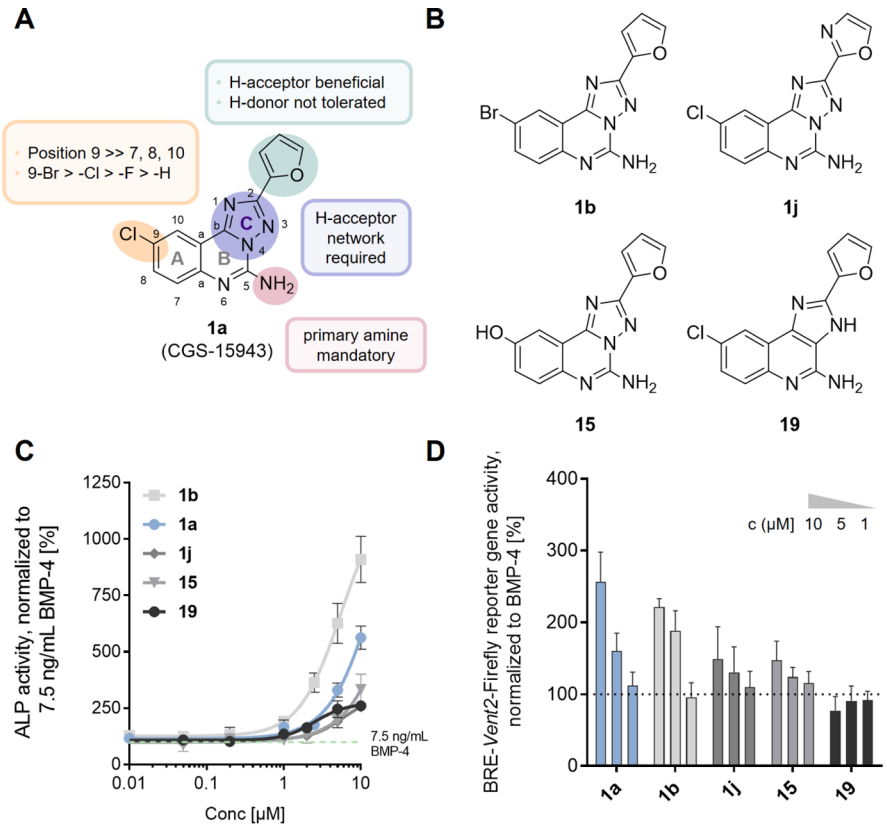

Figure 4. Summary of SARs of triazolo[1,5-*c*]quinazolines as osteogenic BMP signaling amplifiers. (A) Schematic illustration of the BMP amplifier pharmacophore of **1a**. (B) Chemical structures of **1a** derivatives to illuminate key structural features. (C,D) Dose−response profiles on BMP-dependent osteoblast differentiation (% ALP activity, panel C) and the BMP pathway (BRE reporter, panel D). Data are shown as mean ± SD ($n \geq 3$), normalized to BMP-4/DMSO vehicle (= 100%).

this effect could not be "primed" by pre-treatment with **1a** in the absence of BMP-4 (Figure 3E).

In addition, a TGFβ/BMP superfamily-focused qPCR array substantiated that the actual expression of BMP-Smads is not significantly enhanced (Figure S3C−E). Instead, the expression of Smad-dependent BMP target genes is increased (Figure S3E), indicating a mechanism for **1a** that involves an increased and sustained availability of BMP-Smads. Importantly, and in contrast to the reported BMP sensitizers PD-407824 and Chromenone 1 (Scheme 1), BMP-Smads are not enhanced at the expense of TGFβ-Smads.

Together, these data support a unique and therapeutically attractive mode of action for **1a** as a BMP amplifier modality that entails a highly BMP-dependent, enhanced, and sustained action on canonical signaling outputs.

2.3. Design and Synthesis of a Focused Library of Triazolo[1,5-*c*]quinazolines and Scaffold Derivatives. In order to comprehend the unique BMP amplifier efficacy of **1a** and elucidate its mode of action on a molecular basis, we prepared a set of triazolo[1,5-*c*]quinazolines and closely related scaffold derivatives. The focus was on putative pharmacophoric features, including the 2-heteroaryl, 5-amino, and 9-chloro substituents, as well as on the investigation of the heterocyclic core structure. To do this, a synthetic route was devised, which enabled access to a set of diversely substituted triazoloquinazolines and scaffold analogues from a unified reaction path (Scheme 1). Starting from 2-aminobenzonitriles **2a−h**, we modified and combined reported routes that eventually provided several branching points for further diversification.[22−25] Each intermediate of a four-step core sequence (i.e., from **2** over **3**, **4**, and **5** to **1**) served as a starting material for distinct modifications, thereby expanding the diversity of this compound collection at multiple nodes. Employing this route, the original CGS-15943 (**1a**) was prepared in good overall yields (49%, four steps). By using the respective hydrazides in the second step of the synthetic sequence, 2-oxazole **1i** and 2-pyrrole **1j** were obtained.

To characterize the biological relevance of the 5-amino substituent, a series of mono-/bis-alkylated and -acylated derivatives (**6-11d**) were accessible by either direct functionalization of the exocyclic amine (**1**) or reacting suitable amines with 5-chloro precursors (**5**). Moreover, a **1a** derivative was prepared, which lacked the 5-amine. Basic hydrolysis of lactam **4a** furnished a ring-opened, triarylic derivative **12a** that could be re-cyclized with formic acid to yield the desired 5-unsubstituted triazolo[1,5-*c*]quinazoline **13**. When using 9-bromo derivative **4b** for hydrolysis, the stable cyclic aminal **14** formed as a side product during reaction work-up and was isolated for structure−activity relationship (SAR) studies.

In addition to a positional scan of the 9-chloro substituent (i.e., **f−h** series, 7-, 8-, and 10-position), a number of derivatives were prepared, which replaced the 9-chloro (**a**) by bromo- (**b**), fluoro- (**c**), and *O*- and *N*-functionalities. 9-Methoxy derivatives (**e** series) were prepared by the core four-step route. Phenol **15** was furnished with boron tribromide as the demethylation reagent from both **1e** and **5e**. 9-Amine **16** was readily accessible from **5b** via copper-catalyzed dual amination of the 5- and 9-halides with ammonium hydroxide.

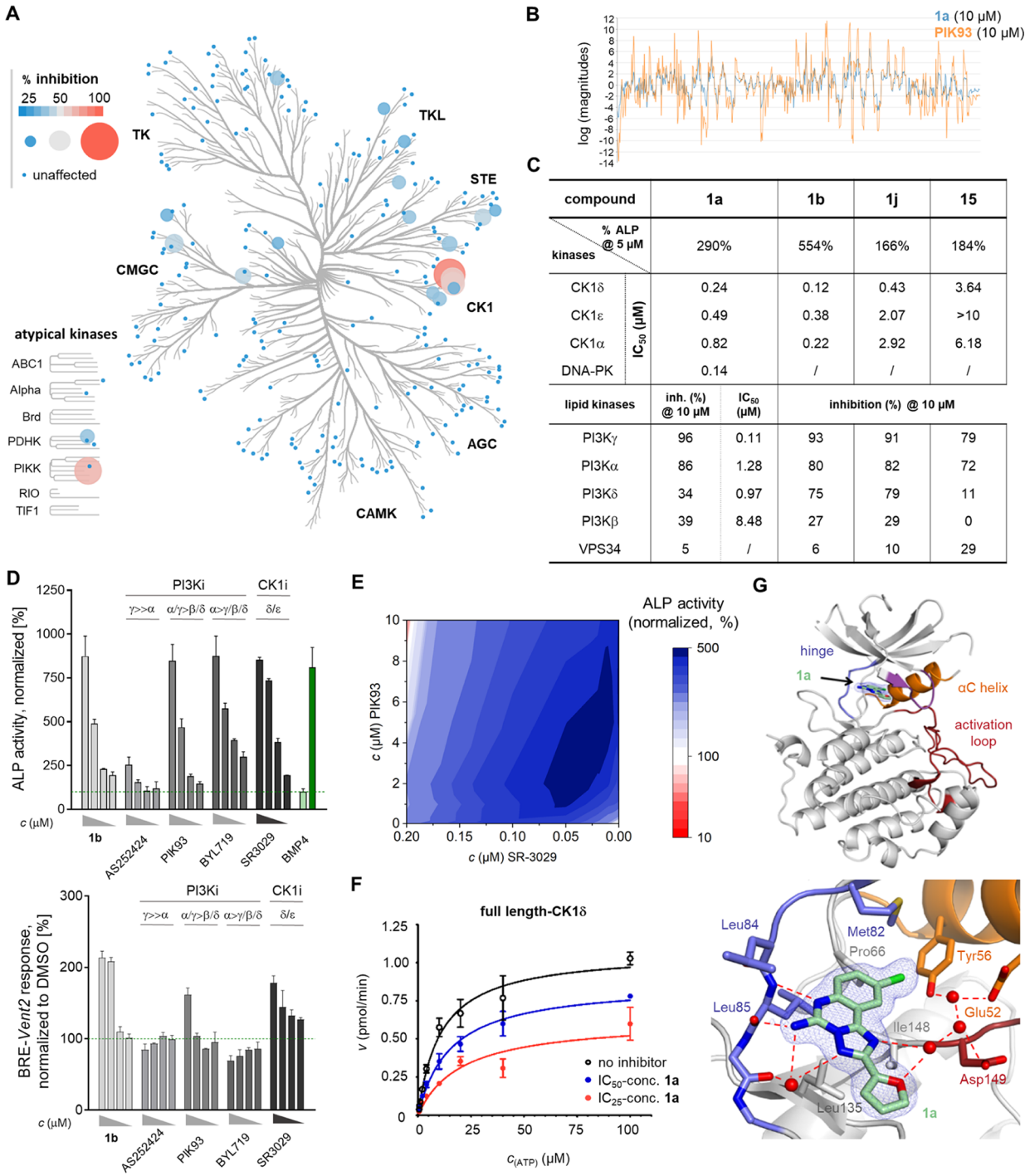

compound		1a		1b	1j	15
kinases \ % ALP @ 5 µM		290%		554%	166%	184%
CK1δ	IC_{50} (µM)	0.24		0.12	0.43	3.64
CK1ε		0.49		0.38	2.07	>10
CK1α		0.82		0.22	2.92	6.18
DNA-PK		0.14		/	/	/
lipid kinases		**inh. (%) @ 10 µM**	**IC_{50} (µM)**	**inhibition (%) @ 10 µM**		
PI3Kγ		96	0.11	93	91	79
PI3Kα		86	1.28	80	82	72
PI3Kδ		34	0.97	75	79	11
PI3Kβ		39	8.48	27	29	0
VPS34		5	/	6	10	29

Figure 5. Kinome screen and Cell Painting assay identify CK1***δ/ε***- and PI3K***α/γ***-isoforms as relevant targets of triazolo[1,5-*c*]quinazolines. (A) Kinome screen of **1a** (1 μM) versus 408 kinases identifies CK1, DNA-PK, and PI3K as putative targets (>50% inhibition, relative to DMSO control); data plotted with CORAL, lipid kinases are not shown. (B) Morphological fingerprints of **1a** and PIK93 in the Cell Painting assay reveal high biosimilarity (83%) with class I PI3K inhibitors. (C) IC_{50} validation and characterization of kinase inhibition profiles by **1a** and a selected set of derivatives, including direct comparison with osteogenic BMP activity from osteoblast differentiation assays in C2C12 cells (% ALP activity). Data are shown as mean ± SD (n = 3). (D) Side-by-side comparison of **1b** with distinct pan-PI3K (PIK93), PI3Kα/γ-selective (AS252424, BYL-719), and CK1δ/ε (SR3029) chemotypes on osteoblast differentiation (% ALP activity, upper panel) and BMP pathway activity (% BRE reporter response, lower panel), normalized to BMP-4/DMSO (= 100%). **1b** and PI3K inhibitors were tested at 0.1, 1, 5, and 10 μM and SR3029 at 0.005, 0.02, 0.1, and 0.2 μM. Data are shown as mean ± SD (n = 3). (E) Titration of CK1δ/ε (SR3029) against pan-PI3K (PIK93) inhibition synergistically enhances BMP-dependent osteoblast differentiation (% ALP activity, normalized to 7.5 ng/mL BMP4). (F) Michaelis–Menten kinetics of 1a against full-length CK1δ reveals a mixed competitive and non-competitive inhibition type. Data are shown as mean ± SD (n = 3). (G) Co-crystal structure of **1a**-bound CK1δ (pdb7NZY) illustrates the binding mode of **1a** within the ATP pocket. Electron density of **1a** is depicted as a blue mesh with a contour level of 1σ (2mFo-Fc map), red dashed lines symbolize stabilizing hydrogen bond interactions, and coordinated water molecules are shown as red spheres.

Albeit **12a,b** and cyclic aminal **14** were already useful to investigate conformational aspects of the rigid **1a** scaffold, a "scaffold hop" was envisioned, which could significantly alter a H-bond network originating from the heterocyclic core. Replacing the annulation site nitrogen *N-4* by carbon would switch the C-ring from a sole H-acceptor (1,3,4-triazole) to a mixed H-donor/acceptor (imidazole), while not qualitatively affecting the 5-aminoquinoline H-bond features (**19**). However, a new synthetic route had to be established for this purpose. Building on previous work,[26,27] the desired imidazo[4,5-*c*]quinoline scaffold (**20**) was built up in four steps from **21**, followed by N-oxidation using *m*-CPBA. Importantly, a Boc group had to be installed at the imidazole ring prior to N-oxidation to overcome the otherwise notoriously low solubility of *N*-oxide **26** (Scheme S1). Next, tosylation of *N*-oxide **28** for CH-activation at the *ortho*-position enabled nucleophilic substitution with ammonia to furnish the desired imidazo[4,5-*c*]quinoline **19**.

2.4. Structure−Activity Relationships Define Pharmacophore Features of Triazolo[1,5-*c*]quinazolines. A total of 39 synthesized CGS-15943 **1a** derivatives and 13 commercially available, structurally related compounds (**C1−C13**) were systematically profiled for their biological activities as osteogenic BMP signaling amplifiers (see Figure S4). Figure 4A summarizes our key findings on structural motifs that appeared essential for activity, defining the pharmacophore. Figure 4B−D depicts dose−response profiles of selected compounds on osteoblastogenesis in C2C12 cells (ALP activity, left panel) and BMP reporter activity (BRE, right panel).

The lack of BMP activity observed for derivative **13** indicated that the 5-amino functionality is mandatory (Figure S4A). Profiling of nine differently mono-/bis-alkylated (**8, 9, 11a−d**) or -acylated (**6, 7, 10**) derivatives confirmed the importance of an unsubstituted 5-amino group (Figure S4A). Replacement of the 5-nitrogen by oxygen (**4a**) or chlorine (**5a**) resulted in a complete loss of activity, and most 5-chloro-substituted derivatives turned out rather problematic due to cytotoxicity (data not shown). We next assessed whether the chlorine can be moved from the 9- to 7-, 8-, or 10-position (**1f−h**), but all regioisomers turned out inactive (Figure S4B). However, a robust increase in BMP activity was monitored from the inactive 9-unsubstituted to 9-fluoro, 9-chloro to 9-bromo derivative (**1a−d**, Figures 4C,D and S4B). Interestingly, both 9-hydroxy (**15**) and 9-amino (**16**) substitution significantly reduced biological activity and most pronounced in the BMP reporter assay (Figure S4C). Replacing the fur-2-yl substituent in the 2-position requires careful selection. A pyrrol-2-yl (**1i**) already diminished activity, whereas oxazol-2-yl **1j** was still active, indicating relevant H-acceptor functions via the heterocyclic oxygen (Figures 4C,D and S4D).

Several scaffold derivatives of **1a** were tested to illuminate essential features of the heterocyclic core. For imidazo[4,5-*c*]quinoline **19**, the 1,3,4-triazole annelant was replaced by imidazole, which strongly reduced osteogenic BMP activity in direct comparison to **1a** and completely abolished activity in the BRE reporter assay (Figures 4C,D and S4E). This finding points at either sole H-bond acceptor qualities required for target engagement or a counterproductive effect of a H-donor in this region of the molecule. Given that already such minor scaffold variations dramatically impact BMP amplifier activity of **1a**, it was not surprising that none of the other scaffold derivatives turned out active (Figure S3E,F). Interestingly, ring-opened, triarylic derivative **12a** (Figure S3E) was similarly effective in C2C12 cells as **1a** but much less active in the BRE reporter assay, pointing at a distinct target profile.

Together, the overall steep SAR and distinct activity profiles in different BMP-dependent assays suggested that more than one cellular target might be responsible for the BMP amplifying mechanism of triazolo[1,5-*c*]quinazolines (see Chapter 2.5).

2.5. Holistic Target Deconvolution Identifies CK1 and PI3K Isoforms as Targets of 1a. In view of our aim to expand the druggable space of small-molecule BMP activator modalities, several target deconvolution strategies were pursued. **1a** has originally been developed as a non-selective adenosine receptor antagonist with sub-micromolar activity against all four receptor types.[28−30] In order to delineate a possible link to BMP signaling, a collection of 45 adenosine receptor antagonists, agonists, and modulators of adenosine metabolism were profiled in all BMP-dependent assays (Figure S5). None of these compounds mirrored the BMP phenotype of **1a** in any of the assays, excluding adenosine-associated effectors as responsible targets. The same was true for the very recently reported activity of **1a** on the aryl hydrocarbon receptor,[31] which we could exclude as a BMP-relevant target compared to the selective AhR activator FICZ (Figure S6A−D).

Although affinity-based pulldown proteomics presents powerful tools for target identification, these approaches were not applicable to **1a**. The SAR study did not identify suitable sites for incorporation of the necessary linkers and/or reactive functionalities. Hence, we followed rather holistic approaches such as the Cell Painting assay (CPA)[32−34] and kinome and transcriptomic profiling in order to dissect putative targets. Screening against 408 kinases unveiled a relatively clean kinome profile for **1a** (i.e., standard selectivity score,[35] S_{50} = 1.23%) since only five kinases were inhibited <50% residual enzyme activity at 1 μM (Figure 5A). These were casein kinase 1 (CK1) α, δ and ε isoforms, the atypical DNA-dependent protein kinase (DNA-PK), and the phosphatidylinositol kinase 3 (PI3K) γ isoform. Morphological fingerprinting by CPA reinforced that PI3K lipid kinases might be a relevant target (Figure 5B). CPA profiling was performed in the well-established osteosarcoma cell line U2OS, thus recapitulating a BMP-relevant cellular context. Notably, U2OS cells have previously been used to assess aspects of Akt/PI3K and CK1 biology.[36,37] PIK93 presents a distinct PI3K inhibitor chemotype compared to **1a** (15% chemical similarity) but displayed a high biosimilarity score of 83%. Dose−response profiling of **1a** further confirmed potent inhibition of these kinases with the highest potencies against PI3Kγ (IC_{50} = 0.11 μM), CK1δ/ε (IC_{50} = 0.24 and 0.49 μM), and DNA-PK (IC_{50} = 0.14 μM) (Figure 5C).

A chemical biology approach was employed to assess and rank the relevance of each kinase in the context of osteogenic BMP signaling. We could exclude DNA-PK as a relevant target early on since two structurally distinct DNA-PK inhibitors (NU7026, AZD7648) were completely inactive in the BMP assays (Figure S6E−G). It should be noted that small-molecule DNA-PK inhibition is generally difficult to discriminate from PI3K inhibition.[38] However, due to its high DNA-PK selectivity, the recently disclosed AZD7648 served as an efficient tool to probe the relevance of this kinase over PI3K isoforms in the context of BMP signaling.[39] In fact, profiling a series of distinct PI3K inhibitors revealed significant

contributions to a BMP amplifying phenotype (Figure 5D, upper panel). While the highly γ-selective PI3K inhibitor (AS252424)[40] showed only a weak osteogenic activity, PIK93 (α/γ-isoform preference, also inhibits δ/β) and BYL719 (α-isoform preference, also inhibits δ/γ) effectively enhanced BMP-dependent osteoblast differentiation. Notably, all PI3K inhibitors were inactive in the BMP-Smad response element (BRE reporter) assay (Figure 5D, lower panel), emphasizing their major impact on non-canonical as opposed to Smad-dependent signaling effects.

These findings are in good agreement with literature reports on the role of class I PI3Ks in the non-canonical BMP pathway during osteogenesis, inter alia by blockade of competing myogenic differentiation, thus promoting osteoblastic differentiation.[41] Indeed, we observed reduced expression of myogenesis-related markers (e.g., *Igf1/Igfr*, *Il6*, *Pdgfb*, and *End*, Figure S3C,E). However, the contributions of individual class I and II PI3K isoforms to bone formation versus degradation or remodeling and the underlying mechanisms are controversially discussed.[42,43] We could previously show that inhibition of VPS34 (i.e., class III PI3K) is counterproductive for osteogenic BMP activation.[4] None of the herein profiled triazolo[1,5-*c*]quinazolines significantly affected VPS34 (Figure 5C).

Importantly, the CK1δ/ε-selective inhibitor SR3029 recapitulated the triazoloquinazolines' BMP profiles in both assays very well (Figure 5D). Its activity could be further enhanced in a dose-dependent fashion when PIK93 or BYL719, but not AS252424, is added (Figure S7A). This synergy turned out highly robust when SR3029 was used at low concentrations (i.e., 10−50 nM) in combination with PIK93 between 1 and 5 μM (Figure 5E, dark-blue area). Hence, these findings strongly supported a dual mode of action, which was further mirrored by the kinase selectivity profiles of **1a** derivatives (Figure 5C). The highest BMP activities were always observed when both CK1δ/ε and PI3Kα/γ are potently inhibited (**1a,b**), and low inhibition of either CK1 or PI3K isoforms could be, at least in part, compensated by each other (**1j**, **15**).

Given that triazolo[1,5-*c*]quinazolines presented a new CK1 inhibitor chemotype and to further rationalize the cellular SAR on a molecular level, the crystal structure of **1a**-bound CK1δ was resolved at 1.85 Å (Figures 5G and S8C, pdb 7NZY). The binding mode of **1a** revealed a dense hydrogen bond network via almost all *N*-atoms of the heterocyclic scaffold (except for *N*-4) and the exocyclic 5-amino group in the hinge binding region as well as a water cluster between Tyr56, Glu52 of the α-C-helix, and Asp149 from the activation loop. The 2-furane was also engaged in this water cluster. These interactions perfectly explained the lack of BMP activity of 2-pyrrole **1i**, those of all derivatives with a substituted 5-amino group (**6**−**11a**−**d**), and the low activity of the closely related imidazo[4,5-*c*]quinoline **19**. The structural data corroborated that only the 9-position accommodates a substituent within the gatekeeper cavity. As it was evident that 9-chloro and -bromo substitution significantly improved CK1 inhibition potency along with cellular BMP activity, we postulate a critical engagement with Tyr56 and its water cluster. Notably, all key interactions for potent CK1δ inhibition of the triazolo[1,5-*c*]quinazolines permitted binding to PI3K as exemplified from docking **1a** into the active sites of PI3Kα/γ (Figure S8C). In fact, there were less steric restrictions and H-bond interactions observed for **1a**-docked PI3K, making CK1 the decisive and SAR-limiting target for this compound class as BMP amplifiers. It should be noted that CK1 and PI3K do not represent typical off-targets for each other, and thus, reported inhibitor chemotypes for each enzyme class usually do not share common pharmacophores.[44] Consequently, CK1 and PI3K would not have been chosen a priori for a target-centric, dual pharmacology strategy and highlight one of the key assets of the herein presented PDD approach.

Moreover, we found that **1a** exhibited unusual enzyme inhibition kinetics (Figure 5F). The kinetics were determined with the full-length proteins and revealed a mixed type of inhibition for CK1δ (i.e., K_m increased, V_{max} decreased), whereas CK1ε followed a classic ATP-competitive inhibition by **1a** (Figure S8B). Full-length CK1α was only very weakly affected by **1a** (Figure S8A). To the best of our knowledge, there is no small-molecule CK1 inhibitor described that exhibits an isoform-specific, mixed-type inhibition, which might underlie the unique selectivity of **1a** for the BMP pathway. In that respect, none of the triazolo[1,5-*c*]-quinazolines and key scaffold derivatives inhibited GSK3β as a common target for BMP/Wnt signaling activation and an effector of numerous pathway crosstalks (Figure S9).[45−47] Interestingly, CK1 has previously been described to physically interact and phosphorylate Smad proteins.[48] Since this interaction has been characterized for the ε-isoform and functionally only within TGFβ signaling, future efforts should decipher similar functions for CK1δ/ε on BMP-Smad dynamics. The unusual, mixed CK1δ inhibition type might even unravel a moonlighting activity of CK1 isoforms in the context of Smad biology.

3. CONCLUSIONS

Phenotypic drug discovery (PDD) followed by conclusive target identification is a powerful approach for the unbiased identification of novel drug candidates, targets, and mechanisms of action that would not have been discovered via target-centric approaches (TDD).[49] PDD has gained increasing interest in recent years and is now in widespread application in drug discovery.[50] Here, we employed a conceptually novel phenotypic screening approach for the discovery of cytokine activators to act as morphogens during development with the aim to identify new-in-class stimulators of the BMP pathway. The identification of triazolo[1,5-*c*]quinazoline **1a** indeed turned out to expand not only the chemical but also druggable space of currently available small-molecule BMP amplifiers. Our data showed that this compound class uniquely amplified BMP signaling by combined targeting of CK1δ/ε and PI3Kα/γ isoforms. While PI3K-mediated effects supported cell context-dependent, non-canonical contributions to osteogenic BMP signaling, CK1δ/ε perturbation enhanced canonical BMP outputs. Importantly, **1a** efficiently stimulated BMP activity in vitro and in vivo without targeting any of the well-recognized effectors, many of which are associated with pathway promiscuity or toxicity-related liabilities (e.g., GSK3β, CHK1). In this regard, **1a** amplified cellular BMP outputs only in the presence of minimal BMP levels, involving a mechanism that enhanced and sustained the availability of BMP-Smads. Intriguingly, cells could not even be "primed" for this activity by **1a** in the complete absence of BMP. As a consequence, **1a** seemed only capable of stimulating signaling where it is spatiotemporally required but possibly not sufficient. This could be the case during tissue homeostasis and regeneration and is particularly attractive to target in the context of bone formation.

Notably, the identification of the unique dual perturbation of specific CK1/PI3K isoforms for highly effective osteogenic BMP amplification is a result of unbiased PDD, highlighting the intrinsic strength of PDD to discover unrecognized polypharmacology signatures. The herein introduced triazolo-[1,5-*c*]quinazolines may not only serve as a novel biochemical tool to study the BMP pathway but also propel and guide the development of lead candidates to explore in vivo efficacy in osteopenic disease models.

EXPERIMENTAL SECTION

Chemistry. *General Information.* Unless otherwise noted, all commercially available compounds were used as provided without further purification. Solvents for chromatography were technical grade. Analytical thin-layer chromatography (TLC) was performed on Macherey-Nagel silica gel polyester plates with F-254 indicator, visualized by irradiation with UV light. Column chromatography was performed using silica gel Merck 60 (particle size 0.040−0.063 mm). Flash column chromatography was performed using silica gel columns (particle size 0.015−0.050 mm) provided by Interchim (Montluçon, France), Teledyne Isco (Axel Semrau GmbH & Co KG, Sprockhövel, Germany), or BÜCHI Labortechnik GmbH (Essen, Germany). Solvent mixtures are understood as volume/volume. ^{1}H NMR and ^{13}C NMR were recorded on Bruker Avance III 400 (400 MHz, Software: Bruker TopSpin 3.6.0) and Bruker Avance II (600 MHz, Software: Topspin 3.2) spectrometers in DMSO or $CDCl_3$. Data are reported in the following order: chemical shift (δ) in ppm; multiplicities are indicated s (singlet), d (doublet), t (triplet), and m (multiplet); coupling constants (J) are given in Hertz (Hz). High-resolution mass spectra were recorded on a micrOTOFII (Software: Bruker Compass for otofSeries, otofControl Version 3.4) mass spectrometer. Chemical yields refer to isolated pure substances unless otherwise noted. The purity of the synthesized compounds was determined by HPLC via calculating the percentage of the product peak integral relative to the sum of all observed peak integrals at 254 nm. The HPLC purity for all synthesized compounds was >95% for biological testing, unless otherwise noted. The detailed procedures for the synthesis of all herein described compounds and intermediates can be found in the extended experimental section of the Supporting Information, along with physical/spectroscopic data for all new compounds. General procedures and representative and key compounds are summarized here:

*General Procedure A for Substituted Ethyl-N-(2-Cyanophenyl)-carbamates (**3a−h**).*[25] A suspension of respective 2-aminobenzonitrile (10−60 mmol, 1.0 equiv) in excess ethyl chloroformate (50−300 mmol, 5−28 mL) was heated under reflux (95 °C) until TLC control exhibited complete conversion (3−13 h). The reaction mixture was cooled to room temperature, and the solvent was evaporated under reduced pressure utilizing toluene as a co-solvent. The crude residue was suspended in a suitable amount of toluene and heated until a clear solution was formed. The solution was cooled to 80 °C, followed by the addition of cyclohexane until the solution became cloudy. The mixture was allowed to cool to room temperature and filtered to yield a crystalline product, which was then dried under reduced pressure. Addition of cyclohexane to the filtrate and storing the mixture under cool conditions overnight forwarded an additional portion of the product. The product was used without further purification unless otherwise stated.

*Ethyl-N-(4-chloro-2-cyanophenyl)carbamate (**3a**).*[25] The general procedure was performed with 2-amino-5-chlorobenzonitrile [9.16 g, 60.03 mmol, 1.0 equiv) and 28 mL of ethyl chloroformate (294.14 mmol, 4.9 equiv)] for 3 h to yield **3a** as colorless crystals (13.02 g, 97%). ^{1}H NMR (400 MHz, DMSO-d_6): δ 9.83 (s, 1H, NH), 7.98 (d, J = 2.4 Hz, 1H, H-10), 7.74 (dd, J = 2.4, 8.8 Hz, 1H, H-8), 7.55 (d, J = 8.8 Hz, 1H, H-7), 4.16 (q, J = 7.2 Hz, 2H, CH_2), 1.25 (t, J = 7.2 Hz, 3H, CH_3) ppm. ^{13}C NMR (101 MHz, DMSO-d_6): δ 153.8 (C-5), 139.7 (C-6a), 133.9 (C-8), 132.4 (C-10), 128.9 (C-9), 126.5 (C-7), 115.5 (C-10b), 108.6 (C-10a), 61.1 (CH_2), 14.3 (CH_3) ppm.

*Ethyl-N-(4-bromo-2-cyanophenyl)carbamate (**3b**).*[51] The general procedure was performed with 2-amino-5-bromobenzonitrile (1.93 g, 9.80 mmol, 1.0 equiv) and 10 mL of ethyl chloroformate (105.05 mmol, 10.7 equiv) for 3 h to yield **3b** as colorless crystals (2.32 g, 88%). ^{1}H NMR (400 MHz, DMSO-d_6): δ 9.85 (s, 1H, NH), 8.09 (d, J = 2.4 Hz, 1H, H-10), 7.86 (dd, J = 2.4, 8.8 Hz, 1H, H-8), 7.47 (d, J = 8.8 Hz, 1H, H-7), 4.15 (q, J = 7.1 Hz, 2H, CH_2), 1.24 (t, J = 7.1 Hz, 3H, CH_3) ppm. ^{13}C NMR (101 MHz, DMSO-d_6): δ 153.8 (C-5), 140.2 (C-6a), 136.8 (C-8), 135.3 (C-10), 126.7 (C-7), 116.7 (C-9), 115.5 (C-10b), 108.9 (C-10a), 61.1 (CH_2), 14.4 (CH_3) ppm.

*General Procedure B for Substituted Dihydrotriazoloquinazolin-5-Ones (**4a−j**).*[25] A solution of the carbamate (**1a−h**, 4−19 mmol, 1.0 equiv) and the respective carbohydrazide (4−19 mmol, 1.0 equiv) in 1-methylpyrrolidin-2-one (NMP, 10−20 mL) under an inert atmosphere was heated to 160 °C under reflux cooling until TLC control exhibited complete conversion (4.5−18 h). The reaction mixture was cooled to room temperature, followed by the addition of an excess of water, to precipitate the product. After stirring for 30 min, the suspension was filtered. The residual solid was thoroughly washed with water and a little amount of isopropyl alcohol and dried in vacuo to give the product in sufficient purities, which was used without further purification unless otherwise stated.

*9-Chloro-2-furan-2-yl-6H-5,6-dihydro[1,2,4]triazolo[1,5-c]-quinazoline-5-one (**4a**).*[24,25] The general procedure was performed with 2.76 g of **3a** (12.29 mmol, 1.0 equiv) and 1.55 g of furan-2-carbohydrazide (12.29 mmol, 1.0 equiv) in 20 mL of NMP for 18 h to yield **4a** as a light-brown solid (3.40 g, 97%). An analytical sample was purified by silica gel flash chromatography [dichloromethane (DCM)/methanol 0 → 10%]. Note: The ^{1}H NMR spectral data differed slightly from the literature reported values.[25] ^{1}H NMR (400 MHz, DMSO-d_6): δ 12.46 (s, 1H, NH), 8.15 (d, J = 2.4 Hz, 1H, H-10), 7.97 (dd, J = 0.8, 1.6 Hz, 1H, H-5′), 7.76 (dd, J = 2.4, 8.8 Hz, 1H, H-8), 7.46 (d, J = 8.8 Hz, 1H, H-7), 7.26 (dd, J = 0.8, 3.2 Hz, 1H, H-3′), 6.74 (dd, J = 1.6, 3.2 Hz, 1H, H-4′) ppm. ^{13}C NMR (100 MHz, DMSO-d_6): δ 156.0 (C-2), 152.2 (C-10b), 145.3 (C-5′), 145.0 (C-2′), 143.5 (C-5), 136.0 (C-6a), 132.7 (C-8), 127.5 (C-9), 123.0 (C-10), 118.1 (C-7), 112.17 (C-3′), 112.16 (C-4′), 111.6 (C-10a) ppm. HRMS (ESI): m/z calcd for $C_{13}H_7N_4O_2Cl$ $[M-H]^-$: 285.0185, found: 285.0182.

*9-Bromo-2-furan-2-yl-6H-5,6-dihydro[1,2,4]triazolo[1,5-c]-quinazoline-5-one (**4b**).* The general procedure was performed with 1.88 g of **3b** (6.99 mmol, 1.0 equiv) and 0.88 g of furan-2-carbohydrazide (6.98 mmol, 1.0 equiv) in 15 mL of NMP for 18 h to yield **4b** as a brown solid (2.31 g, 100%). An analytical sample was purified by silica gel flash chromatography (DCM/methanol 0 → 10%). ^{1}H NMR (400 MHz, DMSO-d_6): δ 12.48 (s, 1H, NH), 8.27 (d, J = 2.3 Hz, 1H, H-10), 7.98 (dd, J = 0.8, 1.7 Hz, 1H, H-5′), 7.88 (dd, J = 2.3, 8.8 Hz, 1H, H-8), 7.39 (d, J = 8.8 Hz, 1H, H-7), 7.26 (dd, J = 0.8, 3.4 Hz, 1H, H-3′), 6.74 (dd, J = 1.8, 3.4 Hz, 1H, H-4′) ppm. ^{13}C NMR (100 MHz, DMSO-d_6): δ 156.0 (C-2), 152.2 (C-10b), 145.4 (C-5′), 145.0 (C-2′), 143.6 (C-5), 136.4 (C-6a), 135.5 (C-8), 126.0 (C-10), 118.4 (C-7), 115.2 (C-9), 112.3 (C-4′), 112.2 (C-3′), 112.1 (C-10a) ppm. HRMS (ESI): m/z calcd for $C_{13}H_7N_4O_2Br$ $[M + Na]^+$: 352.9650, found: 352.9651.

*General Procedure C for Substituted 5-Chlorotriazoloquinazolines (**5a, d−j**).*[24] A two-necked round-bottom flask was charged with the triazoloquinazolinone (**4a**, **d−j**, 1−15 mmol, 1.0 equiv) under an inert atmosphere and placed on an ice bath. On cooling, an excess of freshly distilled phosphoryl chloride ($POCl_3$, 10−50 mL) was added, followed by the careful addition of dry *N*,*N*-diisopropylethylamine (DIPEA, 2−30 mmol, 2.0 equiv).[52] After removal of the ice bath, the mixture was stirred for 0.5 h at ambient temperature. Subsequently, the suspension was heated to reflux (110 °C). As soon as the TLC control showed no further conversion (21−45 h), the dark solution was cooled to room temperature, carefully poured onto chipped ice in a beaker, and stirred for circa 0.5 h while maintaining the temperature below 20 °C. At that time, a voluminous precipitate began to form. The suspension was filtered, and the residual solid was washed with water and dried in vacuo to give the crude product (**5a**, **d−j**), which still contained a fraction of starting material. Since the purification

after the last step of the synthesis route proved to be more effective, the slightly impure products were used without further purification unless otherwise noted.

*5,9-Dichloro-2-(furan-2-yl)-[1,2,4]triazolo[1,5-c]quinazoline (**5a**).*[24] General procedure C was performed with 2.00 g of **4a** (6.98 mmol, 1.0 equiv) and 2.4 mL of dry DIPEA (1.78 g, 13.78 mmol, 2.0 equiv) in 10 mL of $POCl_3$ (16.40 g, 106.97 mmol, 15.3 eq) for 40 h to yield raw **5a** as a tan solid (2.09 g, 98%). An analytical sample was purified by silica gel flash chromatography (DCM/methanol 0 → 10%). ^{1}H NMR (400 MHz, $CDCl_3$-*d*1): δ 8.56 (d, *J* = 2.4 Hz, 1H, H-10), 7.94 (d, *J* = 8.8 Hz, 1H, H-7), 7.80 (dd, *J* = 2.4, 8.8 Hz, 1H, H-8), 7.68 (dd, *J* = 0.8, 1.6 Hz, 1H, H-5′), 7.35 (dd, *J* = 0.8, 3.6 Hz, 1H, H-3′), 6.63 (dd, *J* = 1.6, 3.6 Hz, 1H, H-4′) ppm. ^{13}C NMR (100 MHz, $CDCl_3$-*d*1): δ 157.6 (C-2), 152.0 (C-10b), 145.5 (C-5′), 145.0 (C-2′), 141.5 (C-6a), 136.2 (C-5), 135.4 (C-9), 133.7 (C-8), 129.8 (C-7), 123.7 (C-10), 118.1 (C-10a), 113.8 (C-3′), 112.4 (C-4′) ppm. HRMS (ESI): *m/z* calcd for $C_{13}H_6N_4OCl_2$ $[M + H]^+$: 304.9997, found: 304.9990.

*General Procedure D for Substituted 5-Chlorotriazoloquinazolines (**5b,c**).*[25] A suspension of triazoloquinazolinone (**4b,c**, 5−6 mmol) in 10−15 mL of phenylphosphonic dichloride ($PhPOCl_2$) was heated to 185 °C under reflux cooling (20−22 h). The resulting dark sirup was cooled to ambient temperature and carefully poured into 300 mL of ice water and stirred for not more than 10 min. At that point, a precipitate began to form. The solid was collected by filtration, washed with water, and dried in vacuo. Next, the crude residue was taken up in 100 mL of DCM three times, treated with ultrasound, and filtered. The combined dark filtrates were charged with silica, followed by the evaporation of the solvent. The resulting solid was used for a silica gel flash chromatography (DCM/methanol 0 → 10%) to yield a pure product (**5b,c**).

*9-Bromo-5-chloro-2-(furan-2-yl)-[1,2,4]triazolo[1,5-c]quinazoline (**5b**).* General procedure D was performed with 1.99 g of **4b** (6.01 mmol, 1.0 eq) in 15 mL of $PhPOCl_2$ (20.69 g, 106.09 mmol, 17.4 equiv) for 20 h to yield **5b** as a colorless solid (0.62 g, 30%). ^{1}H NMR (400 MHz, DMSO-d_6): δ 8.56 (d, *J* = 2.2 Hz, 1H, H-10), 8.12 (dd, *J* = 2.3, 8.8 Hz, 1H, H-8), 8.03 (dd, *J* = 0.7, 1.7 Hz, 1H, H-5′), 7.98 (d, *J* = 8.8 Hz, 1H, H-7), 7.38 (dd, *J* = 0.6, 3.4 Hz, 1H, H-3′), 6.79 (dd, *J* = 1.7, 3.4 Hz, 1H, H-4′) ppm. ^{13}C NMR (100 MHz, DMSO-d_6): δ 155.9 (C-2), 151.6 (C-10b), 146.1 (C-5′), 144.6 (C-2′), 141.5 (C-6a), 136.2 (C-5), 135.9 (C-8), 129.9 (C-7), 125.7 (C-10), 121.8 (C-9), 118.6 (C-10a), 113.5 (C-3′), 112.5 (C-4′) ppm. HRMS (ESI): *m/z* calcd for $C_{13}H_6N_4OClBr$ $[M + Na]^+$: 370.9311, found: 370.9314.

*General Procedure E for Substituted Triazoloquinazolin-5-Amines (**1a−j**).* A suspension of the 5-chlorotriazoloquinazoline (**5a−j**, 0.2−1.6 mmol, 1 equiv) in dry tetrahydrofuran (THF, 8−20 mL) was cooled to 0 °C on an ice bath. Subsequently, an excess of ammonia (ca 7 M NH_3 in methanol or concentrated ammonium hydroxide) was slowly added. The resulting mixture was stirred for 5 min, followed by the removal of the ice bath. At that point, the suspension was stirred until TLC control exhibited full conversion (3−23 h). The reaction was quenched by the careful addition of water, which induced the voluminous precipitation of the raw product, while occasional impurities of the previous synthesis step remained dissolved. The crude solid was collected by filtration, washed with water, and dried under reduced pressure to give the product (**1a−j**) in sufficient purities.

*9-Chloro-2-(furan-2-yl)-[1,2,4]triazolo[1,5-c]quinazoline-5-Amine (**1a**).*[24] General procedure E was performed with 501 mg of **5a** (1.64 mmol, 1.0 equiv) and 4 mL of 7 M NH_3 in methanol (28 mmol, 17.1 equiv) in 20 mL of dry THF for 6 h. The reaction was quenched by the addition of 20 mL of water to yield **1a** as a tan solid (260 mg, 55%). An analytical sample was purified by silica gel flash chromatography (DCM/methanol 0 → 10%). ^{1}H NMR (400 MHz, DMSO-d_6): δ 8.18 (d, *J* = 2.4 Hz, 1H, H-10), 8.10 (s, 2H, NH_2), 7.98 (dd, *J* = 0.8, 1.6 Hz, 1H, H-5′), 7.71 (dd, *J* = 2.4, 8.8 Hz, 1H, H-8), 7.58 (d, *J* = 8.8 Hz, 1H, H-7), 7.28 (dd, *J* = 0.8, 3.2 Hz, 1H, H-3′), 6.76 (dd, *J* = 1.6, 3.2 Hz, 1H, H-4′) ppm. ^{13}C NMR (100 MHz, DMSO-d_6): δ 155.6 (C-2), 150.8 (C-10b), 145.2 (C-5′, C-5), 144.9 (C-2′), 143.8 (C-6a), 132.2 (C-8), 126.9 (C-7), 126.8 (C-10a), 122.1 (C-10), 114.1 (C-9), 112.4 (C-3′), 112.2 (C-4′) ppm. HRMS (ESI): *m/z* calcd for $C_{13}H_8N_5OCl$ $[M + H]^+$: 286.0496, found: 286.0493.

*9-Bromo-2-(furan-2-yl)-[1,2,4]triazolo[1,5-c]quinazoline-5-Amine (**1b**).* General procedure E was performed with 200 mg of **5b** (572 μmol, 1.0 equiv) and 2 mL of 7 M NH_3 in methanol (14 mmol, 24.5 equiv) in 15 mL of dry THF for 6 h. The reaction was quenched by the addition of 15 mL of water to yield **1b** as a tan solid (164 mg, 87%). An analytical sample was purified by silica gel flash chromatography (DCM/methanol 0 → 10%). ^{1}H NMR (400 MHz, DMSO-d_6): δ 8.30 (d, *J* = 2.3 Hz, 1H, H-10), 8.06 (s, 2H, NH_2), 7.98 (dd, *J* = 0.8, 1.7 Hz, 1H, H-5′), 7.82 (dd, *J* = 2.4, 8.9 Hz, 1H, H-8), 7.51 (d, *J* = 8.9 Hz, 1H, H-7), 7.28 (d, *J* = 3.4 Hz, 1H, H-3′), 6.76 (dd, *J* = 1.7, 3.4 Hz, 1H, H-4′) ppm. ^{13}C NMR (100 MHz, DMSO-d_6): δ 155.6 (C-2), 150.8 (C-10b), 145.4 (C-5′), 145.3 (C-2′), 145.1 (C-5), 144.2 (C-6a), 135.0 (C-8), 127.2 (C-7), 125.3 (C-10), 114.70 (C-10a), 114.66 (C-9), 112.5 (C-3′), 112.3 (C-4′) ppm. HRMS (ESI): *m/z* calcd for $C_{13}H_8N_5OBr$ $[M + Na]^+$: 329.9990, found: 329.9995.

*Synthesis of Acyl Derivatives **6** and **7**.* To a suspension of **1a** (286 mg, 1.00 mmol, 1.0 equiv) and benzoyl chloride (576 μL, 697 mg, 4.96 mmol, 5.0 equiv) in a 10 mL microwave vessel was carefully added *N,N*-diisopropyl-ethylamine (DIPEA, 1 mL, 742 mg, 5.74 mmol, 5.7 equiv). The vessel was sealed and placed into the microwave apparatus, and the mixture was heated to 125 C for 1 h with rapid stirring. After cooling to ambient temperature, the heterogeneous mother liquor was suspended in diethyl ether (DEE). The organic phase was washed three times with aqueous 0.1 N HCl solution to remove DIPEA and then four times with aqueous NaOH solution (pH ≈ 11), which separated both products. The organic phase was washed with brine dried over sodium sulfate and concentrated to dryness under reduced pressure to give crude **7**, which was recrystallized from ethanol. The main product (**6**) could be isolated by neutralization of the basic aqueous phase with aqueous 0.1 N HCl solution, followed by collection of the precipitated light-yellow solid by filtration, drying in vacuo, and recrystallization from ethyl acetate/acetone (3:1).

*N-(9-chloro-2-(furan-2-yl)-[1,2,4]triazolo[1,5-c]quinazoline-5-yl)-benzamide (**6**).*[53] Yield: 99 mg (25%) of a colorless solid. ^{1}H NMR (400 MHz, DMSO-d_6): δ 11.74 (s, 1H, NH), 8.45 (s, 1H, H-10), 8.09 (d, *J* = 7.3 Hz, 2H, H-3″), 8.05−7.92 (m, 3H, H-5′, H-8, H-7), 7.72 (t, *J* = 7.1 Hz, 1H, H-5″), 7.62 (t, *J* = 7.6 Hz, 2H, H-4″), 7.33 (d, *J* = 3.1 Hz, 1H, H-3′), 6.75 (dd, *J* = 1.6, 3.2 Hz, 1H, H-4′) ppm. ^{13}C NMR (100 MHz, DMSO-d_6): δ 166.1 (C-1″), 155.8 (C-2), 151.5 (C-10b), 145.7 (C-5′), 144.8 (C-2′), 141.0 (C-6a), 139.0 (C-5), 133.0 (C-8, C-5″), 132.5 (C-2″), 132.3 (C-9), 129.7 (C-7), 128.7 (2x C-4″), 128.5 (2x C-3″), 122.6 (C-10), 117.4 (C-10a), 113.1 (C-3′), 112.3 (C-4′) ppm. HRMS (ESI): *m/z* calc. for $C_{20}H_{12}N_5O_2Cl$ $[M + Na]^+$: 412.0577, found: 412.0575.

*N-Benzoyl-N-(9-chloro-2-(furan-2-yl)-[1,2,4]triazolo[1,5-c]-quinazoline-5-yl)benzamide (**7**).* Yield: 44.4 mg (9%) of a brown crystalline solid. ^{1}H NMR (400 MHz, DMSO-d_6): δ 8.45 (d, *J* = 2.2 Hz, 1H, H-10), 7.97 (dd, *J* = 0.7, 1.7 Hz, 1H, H-5′), 7.93 (dd, *J* = 2.4, 8.8 Hz, 1H, H-8), 7.90−7.84 (m, 5H, H-3″, H-7), 7.65 (t, *J* = 7.5 Hz, 2H, H-5″), 7.51 (t, *J* = 7.8 Hz, 4H, H-4″), 7.32 (dd, *J* = 0.6, 3.5 Hz, 1H, H-3′), 6.75 (dd, *J* = 1.8, 3.5 Hz, 1H, H-4′) ppm. ^{13}C NMR (100 MHz, DMSO-d_6): δ 170.8 (2 × C-1″), 156.7 (C-2), 151.7 (C-10b), 146.3 (C-5′), 144.2 (C-2′), 140.3 (C-6a), 139.0 (C-5), 134.2 (C-9), 134.0 (2 × C-5″), 133.6 (C-8), 132.4 (2 × C-2″), 130.1 (C-7), 129.4 (4 × C-4″), 129.0 (4 × C-3″), 122.9 (C-10), 117.5 (C-10a), 114.1 (C-3′), 112.5 (C-4′) ppm. HRMS (ESI): *m/z* calcd for $C_{27}H_{16}N_5O_3Cl$ $[M + H]^+$: 494.1020, found: 494.1017.

*Methylation of **1a** (**8**, **9**).* To a suspension of **1a** (400 mg, 1.40 mmol, 1.0 equiv) and tetrabutylammonium bromide (TBAB, 1.13 g, 3.51 mmol, 2.5 equiv) in 28 mL of THF on an ice bath, 317 mg of sodium hydride was carefully added (60% dispersion in mineral oil, 7.93 mmol, 5.7 equiv) in portions. After stirring for 10 min, methyl iodide was carefully added to the mixture (215 μL, 490 mg, 3.45 mmol, 2.5 equiv), followed by the removal of the ice bath. Subsequently, the orange mixture was stirred for 4 h at ambient

temperature. The mother liquor was filtrated to separate the solid TBAB. The filtrate was evaporated in vacuo to give the crude mixture of both products, which was taken up in DCM. The organic phase was washed with water twice and once with brine, dried with sodium sulfate, and directly charged with silica before the solvent was removed by evaporation. The residual solid was used for silica gel flash chromatography (cyclohexane/ethyl acetate 10 → 100%) to yield **8** (main product) and **9** (side product) as colorless solids.

*9-Chloro-N,N-dimethyl-2-(furan-2-yl)-[1,2,4]triazolo[1,5-c]-quinazoline-5-Amine (**8**).*[24] Yield: 201.1 mg (46%). ^{1}H NMR (400 MHz, $CDCl_3$-*d*1): δ 8.41 (d, J = 2.4 Hz, 1H, H-10), 7.67 (d, J = 8.8 Hz, 1H, H-7), 7.66 (d, J = 0.4, 1.6 Hz, 1H, H-5′), 7.60 (dd, J = 2.4, 8.8 Hz, 1H, H-8), 7.26 (dd, J = 0.4, 3.2 Hz, 1H, H-3′), 6.62 (dd, J = 1.6, 3.2 Hz, 1H, H-4′), 3.55 (s, 6H, H-1″) ppm. ^{13}C NMR (100 MHz, $CDCl_3$-*d*1): δ 156.1 (C-2), 153.6 (C-10b), 145.9 (C-5), 145.8 (C-2′), 144.7 (C-5′), 142.9 (C-6a), 132.9 (C-8), 129.8 (C-9), 127.4 (C-7), 123.3 (C-10), 115.2 (C-10a), 112.3 (C-3′), 112.1 (C-4′), 41.0 (C-1″) ppm. HRMS (ESI): *m/z* calcd for $C_{15}H_{12}N_5OCl$ [M + H]$^+$: 314.0809, found: 314.0808.

*9-Chloro-2-(furan-2-yl)-N-methyl-[1,2,4]triazolo[1,5-c]-quinazoline-5-Amine (**9**).*[24] Yield: 29.4 mg (7%). ^{1}H NMR (400 MHz, DMSO-d_6): δ 8.07 (d, J = 2.4 Hz, 1H, H-10), 7.96 (dd, J = 0.8, 1.8 Hz, 1H, H-5′), 7.76 (dd, J = 2.4, 9.0 Hz, 1H, H-8), 7.55 (d, J = 9.1 Hz, 1H, H-7), 7.51 (s, 1H, NH), 7.24 (dd, J = 0.8, 3.4 Hz, 1H, H-3′), 6.74 (dd, J = 1.8, 3.4 Hz, 1H, H-4′), 3.73 (s, 3H, CH_3) ppm. ^{13}C NMR (100 MHz, DMSO-d_6): δ 155.8 (C-2), 147.9 (C-10b), 145.3 (C-5′), 144.8 (C-2′), 144.3 (C-5), 137.9 (C-6a), 132.9 (C-8), 126.0 (C-9), 123.3 (C-10), 117.1 (C-7), 112.2 (C-3′, 4′), 111.0 (C-10a), 32.0 (CH_3) ppm. HRMS (ESI): *m/z* calcd for $C_{14}H_{10}N_5OCl$ [M + H]$^+$: 300.0652, found: 300.0649.

*tert-Butyl-N-(9-chloro-2-(furan-2-yl)-[1,2,4]triazolo[1,5-c]-quinazoline-5-yl)carbamate (**10**).*[53] To a stirred solution of **1a** (476 mg, 1.67 mmol, 1.0 equiv) in THF (18 mL) were added solutions of di-*tert*-butyl dicarbonate (749 mg, 3.43 mmol, 2.0 equiv) and, subsequently, *N,N*-dimethyl-pyridin-4-amine (DMAP, 6.5 mg, 53 μmol, 0.03 equiv) in 2 mL of THF, respectively. The resulting mixture was refluxed for 1 h. After cooling to ambient temperature, the mother liquor was diluted with 20 mL of THF and charged with silica, followed by the removal of the solvent by evaporation. The residual solid was used for a silica gel flash chromatography (cyclohexane/ethyl acetate 0 → 100%). A second flash chromatography run (DCM/methanol 0 → 10%) gave pure **10** (403 mg, 63%) as a colorless solid. ^{1}H NMR (400 MHz, DMSO-d_6): δ 10.36 (s, 1H, NH), 8.37 (m, 1H, H-10), 8.01 (dd, J = 0.8, 1.7 Hz, 1H, H-5′), 7.91 (m, 2H, H-7, H-8), 7.33 (dd, J = 0.7, 3.4 Hz, 1H, H-3′), 6.78 (dd, J = 1.8, 3.4 Hz, 1H, H-4′), 1.51 (s, 9H, H-3″) ppm. ^{13}C NMR (100 MHz, DMSO-d_6): δ 155.5 (C-2), 151.2 (C-10b), 150.1 (C-1″), 145.7 (C-5′), 144.9 (C-2′), 141.4 (C-6a), 138.1 (C-5), 132.8 (C-8), 131.2 (C-9), 129.3 (C-7), 122.4 (C-10), 116.7 (C-10a), 112.9 (C-3′), 112.4 (C-4′), 81.4 (C-2″), 27.7 (C-3″) ppm. HRMS (ESI): *m/z* calcd for $C_{18}H_{16}N_5O_3Cl$ [M + H]$^+$: 386.1020, found: 386.1020.

*General Procedure F for the Amination of **5a** (**11a–d**).* A 10 mL microwave vessel was charged with **3a** (110–150 mg, 361–492 μmol) and an excess of the respective amine (0.5–1 mL, 12–22 equiv). The vessel was sealed and placed into the microwave apparatus, and the mixture was heated to the temperature mentioned below for 15 min with rapid stirring. The respective crude products were purified as indicated in the subsections below.

*9-Chloro-2-(furan-2-yl)-N-(prop-2-yn-1-yl)-[1,2,4]triazolo[1,5-c]-quinazoline-5-Amine (**11c**).* General procedure F was performed with 110 mg of **5a** (361 μmol, 1.0 equiv) and 500 μL of propargylamine (430 mg, 7.81 mmol, 21.7 equiv) at 80 °C for 15 min. After cooling to ambient temperature, the heterogeneous mother liquor was taken up in ethyl acetate, washed three times with a 0.1 N ammonium chloride solution (pH ca 5) and once with brine, and dried over sodium sulfate, followed by the removal of the solvents under reduced pressure to yield **11c** (62 mg, 53%) as a yellow solid. ^{1}H NMR (400 MHz, DMSO-d_6): δ 8.78 (t, J = 6.4 Hz, 1H, NH), 8.19 (d, J = 1.6 Hz, 1H, H-10), 7.99 (s, 1H, H-5′), 7.73 (dd, J = 2.0, 8.8 Hz, 1H, H-8), 7.68 (d, J = 8.8 Hz, 1H, H-7), 7.29 (d, J = 3.20 Hz, 1H, H-3′), 6.77 (s, 1H, H-4′), 4.34 (d, J = 4.0 Hz, 2H, H-1″), 3.15 (s, 1H, H-3″) ppm. ^{13}C NMR (100 MHz, DMSO-d_6): δ 155.7 (C-2), 150.8 (C-10b), 145.4 (C-5′), 145.1 (C-2′), 143.2 (C-6a), 142.9 (C-5), 132.4 (C-8), 127.6 (C-7), 127.5 (C-9), 122.2 (C-10), 114.3 (C-10a), 112.5 (C-3′), 112.2 (C-4′), 81.0 (C-2″), 73.1 (C-3″), 30.1 (C-1″) ppm. HRMS (ESI): *m/z* calcd for $C_{16}H_{10}N_5OCl$ [M + H]$^+$: 324.0647, found: 324.0646.

*General Procedure G for B-Ring Cleavage (**12a, b**).*[25] **4a/b** (0.5–10 mmol, 1.0 eq) was suspended in ethylene glycol (20–25 mL) and heated to 100 °C with stirring. Subsequently, aqueous NaOH solution was added to the suspension, and the resulting mixture was heated to 135 °C under reflux cooling until TLC control showed complete conversion (17–43 h). Next, the mother liquor was cooled to ambient temperature, neutralized with diluted HCl solution, and diluted with water and brine, followed by the extraction of the aqueous phase with ethyl acetate. The combined organic phases were washed with brine, dried over sodium sulfate, and evaporated to dryness to give a crude product. Finally, the residue was purified by silica gel chromatography to yield a pure product.

*4-Chloro-2-(3-(furan-2-yl)-1H-1,2,4-triazol-5-yl)aniline (**12a**).*[25] General procedure G was performed with 2.88 g of **4a** (10.05 mmol, 1.0 equiv) and 4 mL of aqueous 5 N NaOH solution (20 mmol, 2.0 equiv) in 25 mL of ethylene glycol for 17 h. Purification by silica gel flash chromatography (cyclohexane/ethyl acetate 60:40%) was used to yield pure **12a** (781 mg, 30%) as a yellow solid. Note: ^{1}H NMR spectra display isomeric signals (ratio ca 48:52) marked with an asterix. Due to their almost equal intensity, a definite distinction between the signals of each isomer was not possible. ^{1}H NMR (400 MHz, DMSO-d_6): δ 14.71 (s, 1H, NH), 14.40 (s, 1H, NH*), 7.98 (d, J = 0.8 Hz, 1H, H-5′), 7.95 (d, J = 2.8 Hz, 1H, H-10), 7.84 (d, J = 2.4 Hz, 1H, H-10*), 7.82 (s, 1H, H5'*), 7.22–7.20 (m, 2H, H-8, H-3′), 7.13 (dd, J = 2.4, 8.8 Hz, 1H, H-8*), 7.03 (d, J = 3.2 Hz, 1H, H-3'*) 6.97 (s, 2H, NH_2), 6.89 (d, J = 9.2 Hz, 1H, H-7), 6.83 (d, J = 8.8 Hz, 1H, H-7*), 6.75 (dd, J = 2.0, 3.2 Hz, 1H, H-4′), 6.50 (dd, J = 1.6, 3.2 Hz, 1H, H-4'*), 6.59 (s, 2H, NH_2*) ppm. ^{13}C NMR (100 MHz, DMSO-d_6): δ 160.9 (C-2), 153.9 (C-10b, C-10b*), 146.3 (C-2*), 146.2 (C-2′), 146.0 (C-6a), 145.5 (C-6a*), 145.1 (C-5'*), 143.7 (C-5′), 142.5 (C-2'*), 130.7 (C-8), 129.2 (C-8*), 126.9 (C-10*), 126.0 (C-10), 118.4 (C-9, C-9*), 118.0 (C-7*), 117.4 (C-7), 113.3 (C-10a), 112.3 (C-4'*), 111.6 (C-4′), 111.2 (C-3'*), 109.1 (C-3′), 108.4 (C-10a*) ppm. HRMS (ESI): *m/z* calcd for $C_{12}H_9N_4OCl$ [M + H]$^+$: 259.0392, found: 259.0385.

*4-Bromo-2-(3-furan-2-yl-1H-1,2,4-triazol-5-yl)aniline (**12b**).* General procedure G was performed with 165.6 mg of **4b** (499 μmol, 1.0 equiv) and 1.5 mL of 1 N aqueous NaOH solution (1.5 mmol, 3.0 equiv) in 20 mL of ethylene glycol for 43 h. A first purification by silica gel chromatography (DCM/ethyl acetate 0 → 25%) to separate the designated product from side products gave 53.3 mg of **6b**, showing two main isomers in the ^{1}H NMR spectra (ca 1:1) and some minor impurities (<10%). The product fraction was taken up in DCM and charged with silica, and the solvents were evaporated. The residual solid was used for a second silica gel flash chromatography run (DCM/ethyl acetate 0 → 15%), resulting in a mixture of pure **12b** and a completely new side product, which was finally separated by semipreparative reverse-phase (RP) HPLC (H_2O/ACN, 10 → 90%) to yield **6b** (3 mg, 2%) as a colorless solid. ^{1}H NMR (400 MHz, DMSO-d_6): δ 14.51 (s, 1H, NH), 8.01 (d, J = 1.0 Hz, 1H, H-10), 7.89 (s, 1H, H-5′), 7.27 (dd, J = 2.2, 8.8 Hz, 1H, H-8), 7.13 (s, 1H, H-3′), 6.80 (d, J = 8.8 Hz, 3H, H-7, NH_2), 6.70 (s, 1H, H-4′) ppm. ^{13}C NMR (100 MHz, DMSO-d_6): δ 159.4 (C-2), 146.1 (C-6a), 144.4 (C-2′), 144.3 (C-5′), 144.2 (C-10b), 132.7 (C-8), 129.3 (C-10), 118.1 (C-7), 112.0 (C-4′), 110.2 (C-3′), 105.6 (C-10a, C-9) ppm. HRMS (ESI): *m/z* calcd for $C_{12}H_9N_4OBr$ [M + H]$^+$: 305.0038, found: 305.0030.

*9-Bromo-2-furan-2-yl-5,5-dimethyl-5,6-dihydro[1,2,4]triazolo-[1,5-c]quinazoline (**14**).* Dihydrotriazolo-quinazoline **14** was identified as the side product resulting from the second flash purification of **12b** (see above) and was isolated by semipreparative RP HPLC (H_2O/ACN, 10 → 90%). Yield: 6.9 mg (4%); ^{1}H NMR (400 MHz, DMSO-d_6): δ 7.82 (dd, J = 0.8, 1.7 Hz, 1H, H-5′), 7.75 (d, J = 2.4 Hz,

1H, H-10), 7.43 (dd, J = 2.3, 8.7 Hz, 1H, H-8), 7.40 (s, 1H, NH), 6.99 (dd, J = 0.7, 3.3 Hz, 1H, H-3′), 6.81 (d, J = 8.7 Hz, 1H, H-7), 6.65 (dd, J = 1.8, 3.4 Hz, 1H, H-4′), 1.70 (s, 6H, 1″) ppm. ^{13}C NMR (100 MHz, DMSO-d_6): δ 154.5 (C-2), 147.6 (C-10b), 146.0 (C-2′), 143.9 (C-5′), 141.7 (C-6a), 134.4 (C-8), 125.8 (C-10), 117.0 (C-7), 111.8 (C-4′), 111.2 (C-10a), 109.5 (C-3′), 108.9 (C-9), 73.3 (C-5), 27.8 (2x C-1″) ppm. HRMS (ESI): m/z calcd for $C_{15}H_{13}N_4OBr$ $[M + H]^+$: 345.0351, found: 345.0354.

*9-Chloro-2-(furan-2-yl)-[1,2,4]triazolo[1,5-c]quinazoline (**13**).* 230 mg of **12a** (0.88 mmol, 1.0 equiv) was suspended in 5 mL of formic acid and heated to reflux (110 °C) for 16 h. After cooling to ambient temperature, the mother liquor was neutralized with 5 N aqueous NaOH solution, which resulted in the precipitation of the product. The solid was collected by filtration, dried in vacuo, and recrystallized from ethyl acetate to yield pure **13** (210 mg, 88%) as yellow crystals. ^{1}H NMR (400 MHz, $CDCl_3$-$d1$): δ 9.67 (s, 1H, H-5), 8.48 (d, J = 2.4 Hz, 1H, H-10), 8.12 (d, J = 8.8 Hz, 1H, H-7), 8.03–7.96 (m, 2H, H-5′, H-8), 7.33 (dd, J = 0.6, 3.5 Hz, 1H, H-3′), 6.77 (dd, J = 1.7, 3.4 Hz, 1H, H-4′) ppm. ^{13}C NMR (100 MHz, $CDCl_3$-$d1$): δ 156.6 (C-2), 149.8 (C-10b), 145.7 (C-5′), 145.0 (C-2′), 141.2 (C-6a), 139.4 (C-5), 133.4 (C-9), 132.6 (C-8), 130.7 (C-7), 122.4 (C-10), 118.7 (C-10a), 112.8 (C-3′), 112.3 (C-4′) ppm. HRMS (ESI): m/z calcd for $C_{13}H_7N_4OCl$ $[M + Na]^+$: 293.0206, found: 293.0211.

*2-(Furan-2-yl)-9-hydroxy-[1,2,4]triazolo[1,5-c]quinazoline-5-Amine (**15**).* To an ice-cooled solution of **1e** (58.2 mg, 207 μmol, 1.0 equiv) in 15 mL of dry DCM under an inert atmosphere was added 0.8 mL of a 1 M bortribromide solution in DCM (800 μmol, 3.9 equiv). After removal of the ice bath, the mixture was protected from sunlight and stirred for 96 h at ambient temperature. Subsequently, the solution was refluxed for another 24 h. Next, the reaction was cooled to 0 °C and quenched by the addition of 500 μL of methanol. The resulting solution was poured onto ice water and extracted with DCM (4 × 50 mL). Throughout the extraction process, a fine precipitate started to form in the aqueous phase, which was collected by filtration. The combined organic phases were dried over sodium sulfate and reduced to dryness by evaporation. The residue was combined with the solid isolated from the aqueous phase and purified by silica gel flash chromatography (DCM/methanol 0 → 10%) to yield pure **15** (10.0 mg, 18%) as a colorless solid. ^{1}H NMR (400 MHz, DMSO-d_6): δ 9.84 (s, 1H, OH), 7.96 (dd, J = 0.8, 1.7 Hz, 1H, H-5′), 7.53 (s, 1H, NH2), 7.48 (d, J = 2.7 Hz, 1H, H-10), 7.46 (d, J = 8.9 Hz, 1H, H-7), 7.26 (dd, J = 0.8, 3.4 Hz, 1H, H-3′), 7.21 (dd, J = 2.8, 8.9 Hz, 1H, H-8), 6.75 (dd, J = 1.8, 3.4 Hz, 1H, H-4′) ppm. ^{13}C NMR (100 MHz, DMSO-d_6): δ 155.3 (C-2), 153.4 (C-9), 151.3 (C-10b), 145.5 (C-2′), 145.1 (C-5′), 142.9 (C-5), 138.4 (C-6a), 126.4 (C-7), 122.4 (C-8), 113.7 (C-10a), 112.2 (C-4′), 112.0 (C-3′), 106.1 (C-10) ppm. HRMS (ESI): m/z calcd for $C_{13}H_9N_5O_2$ $[M + H]^+$: 268.0834, found: 268.0830.

*2-Furan-2-yl-[1,2,4]triazolo[1,5-c]quinazoline-5,9-diamine (**16**).* 5-chlorotriazolquinazoline **5b** (106.2 mg, 304 μmol, 1.0 equiv) was weighed in a 50 mL reaction vessel with a screw cap and suspended in 20 mL of concentrated NH_4OH. 77.1 mg of copper sulfate pentahydrate (309 μmol, 1.0 equiv) was added in one portion; the vessel was sealed, and the suspension was heated to 140 °C for 6 days. The mixture was cooled to ambient temperature, and the solvent was evaporated under reduced pressure. Subsequently, the resulting dark residue was taken up in 12 mL of 2 N aqueous HCl solution and stirred for 4 h at ambient temperature. The suspension was basified with saturated $NaHCO_3$ solution and extracted with DCM (5 × 40 mL). The combined organic phases were dried over sodium sulfate and reduced to dryness. The solvent from the aqueous phase, which still contained a fraction of product, was evaporated. The residue was taken up with THF, treated with ultrasound, and filtrated, and the filtrate was dried in vacuo. Both crude residues were combined and purified by silica gel flash chromatography (DCM/methanol 1 → 10%) to yield **16** (13 mg, 16%) as a tan solid. An analytical sample was purified by semipreparative RP HPLC (H_2O/ACN, 10 → 90%). ^{1}H NMR (400 MHz, DMSO-d_6): δ 7.95 (dd, J = 0.8, 1.7 Hz, 1H, H-5′), 7.35–7.28 (m, 4H, H-1″, H-7, H-10), 7.23 (dd, J = 0.8, 3.4 Hz, 1H, H-3′), 7.05 (dd, J = 2.6, 8.8 Hz, 1H, H-8), 6.74 (dd, J = 1.8, 3.4 Hz, 1H, H-4′), 5.41 (s, 2H, H-2″) ppm. ^{13}C NMR (101 MHz, DMSO-d_6): δ 155.2 (C-2), 151.3 (C-10b), 145.8 (C-2′), 145.1 (C-9), 145.0 (C-5′), 142.0 (C-5), 136.3 (C-6a), 125.8 (C-7), 121.7 (C-8), 114.0 (C-10a), 112.2 (C-4′), 111.8 (C-3′), 103.9 (C-10) ppm. HRMS (ESI): m/z calcd for $C_{13}H_{10}N_6O$ $[M + H]^+$: 267.0994, found: 267.0995.

*9-Chloro-6-methyl-2-(pyrrol-2-yl)-6H-5,6-dihydro[1,2,4]triazolo-[1,5-c]quinazoline-5-one (**17**).* A suspension of 456.3 mg of **5i** (1.50 mmol, 1.0 equiv) in 15 mL of dry THF under an inert atmosphere was placed on an ice bath. Subsequently, 155.6 mg of sodium hydride (60% dispersion in mineral oil, 3.89 mmol, 2.6 equiv) was carefully added in portions, and the mixture was stirred at 0 °C for 10 min. After the addition of 120 μL of methyl iodide (273.6 mg, 1.93 mmol, 1.3 equiv), the ice bath was removed. The resulting suspension was stirred for 22 h at ambient temperature. The reaction was quenched by the filtration of the mother liquor. The filtrate was charged with silica, the solvent was evaporated, and the resulting solid was used for silica gel flash chromatography (cyclohexane/ethyl acetate 25 → 100%) to yield **17** as a light-yellow solid (73 mg, 16%). An analytical sample was purified by semipreparative RP HPLC (H_2O/ACN, 10 → 90%). ^{1}H NMR (400 MHz, DMSO-d_6): δ 11.96 (s, 1H, H-1′), 8.21 (d, J = 2.5 Hz, 1H, H-10), 7.86 (dd, J = 2.5, 9.1 Hz, 1H, H-8), 7.73 (d, J = 9.1 Hz, 1H, H-7), 6.98–6.93 (m, 1H, H-5′), 6.88–6.83 (m, 1H, H-3′), 6.24–6.19 (m, 1H, H-4′), 3.73 (s, 3H, CH_3) ppm. ^{133}C NMR (100 MHz, DMSO-d_6): δ 158.5 (C-2), 150.9 (C-10b), 144.3 (C-5), 137.1 (C-6a), 132.6 (C-8), 127.9 (C-9), 123.3 (C-10), 121.9 (C-5′), 121.8 (C-2′), 118.2 (C-7), 112.3 (C-10a), 110.7 (C-3′), 109.4 (C-4′), 31.4 (CH_3) ppm. HRMS (ESI): m/z calcd for $C_{14}H_{10}N_5OCl$ $[M + Na]^+$: 322.0472, found: 322.0467.

*2-(Furan-2-yl)-9-hydroxy-6H-5,6-dihydro[1,2,4]triazolo[1,5-c]-quinazoline-5-one (**18**).* Pyridinium chloride (15.0 g, 129 mmol) was weighed in a round-bottom flask and heated to 170 °C. At that point, **5e** (57 mg, 190 μmol, 1.0 equiv) was added in portions to the molten mass. The resulting solution was stirred for 4.5 h. Next, the mixture was cooled to ambient temperature, resulting in its solidification. The residue was dissolved in 25 mL of water and acidified with 1 M aqueous HCl solution (pH 2–3), inducing the precipitation of the product. The solid was collected by filtration and dried in vacuo to yield **18** (45 mg, 89%) as a colorless solid. An analytical sample was purified by silica gel flash chromatography (DCM/methanol 0 → 10%). Note: Although this has not been experimentally further confirmed, we believe that hydrolysis of the 5-chloro substituent during this reaction was due to residual water from the starting material **5e**. ^{1}H NMR (400 MHz, DMSO-d_6): δ 12.14 (s, 1H, NH), 9.95 (s, 1H, OH), 7.96 (dd, J = 0.8, 1.8 Hz, 1H, H-5′), 7.48 (d, J = 2.8 Hz, 1H, H-10), 7.31 (d, J = 8.9 Hz, 1H, H-7), 7.25 (dd, J = 0.7, 3.4 Hz, 1H, H-3′), 7.18 (dd, J = 2.8, 8.9 Hz, 1H, H-8), 6.73 (dd, J = 1.7, 3.4 Hz, 1H, H-4′) ppm. ^{133}C NMR (100 MHz, DMSO-d_6): δ 155.9 (C-2), 153.5 (C-9), 153.0 (C-10b), 145.24 (C-2′), 145.19 (C-5′), 143.5 (C-5), 130.0 (C-6a), 122.0 (C-8), 117.6 (C-7), 112.1 (C-4′), 111.9 (C-3′), 110.8 (C-10a), 107.8 (C-10) ppm. HRMS (ESI): m/z calcd for $C_{13}H_8N_4O_3$ $[M + Na]^+$: 291.0494, found: 291.0493.

*Synthesis of Imidazo[4,5-c]quinoline **19**. 6-Chloroquinoline-3,4-diamine (**24**).*[54] A mixture of **23** (301 mg, 1.35 mmol, 1,0 equiv) and sodium dithionite was suspended in 45 mL of EtOH, followed by the addition of 15 mL of water. The reaction mixture was heated to reflux (95 °C) for 1 h. After cooling to ambient temperature, the colorless solid was separated by filtration and washed with EtOH. The light-yellow filtrate was diluted with 25 mL of water, followed by the evaporation of the organic solvent under reduced pressure. The resulting aqueous phase was basified using saturated sodium bicarbonate solution and extracted with ethyl acetate. The combined organic phase was dried over sodium sulfate, followed by the evaporation of the solvent. The resulting solid was dried in vacuo to give **24** (207 mg, 79%) as a dark-yellow solid. ^{1}H NMR (400 MHz, DMSO-d_6): δ 8.20 (s, 1H, H-5), 8.10 (d, J = 2.3 Hz, 1H, H-10), 7.64 (d, J = 8.9 Hz, 1H, H-7), 7.28 (dd, J = 2.3, 8.9 Hz, 1H, H-8), 5.91 (s, 2H, NH_2), 4.89 (s, 2H, NH_2) ppm. ^{133}C NMR (100 MHz, DMSO-d_6): δ 141.4, 141.1, 132.9, 131.0, 128.1, 126.0, 124.6, 120.0, 119.3

ppm. LC−MS (ESI): m/z = 193.9 (100%, ^{35}Cl) $[M + H]^+$, 195.9 (31%, ^{37}Cl) $[M + H]^+$.

*Sodium Furan-2-yl(hydroxy)methanesulfonate (**25**).*[55] A solution of furfural (3.90 mL, 4.52 g, 47.09 mmol) in 75 mL of MeOH was stirred at ambient temperature for 10 min, followed by the addition of 10 mL of freshly prepared saturated aqueous solution of sodium metabisulfite. After stirring at ambient temperature for further 15 min, the cloudy suspension was stored in a freezer overnight. The resulting solid was separated by filtration and dried in vacuo to give **25** (7.30 g, 74%) as a beige solid. ^1H NMR (400 MHz, DMSO-d_6): δ 7.51 (dd, J = 1.2, 1.6 Hz, 1H, H-5′), 6.37−6.33 (m, 2H, H-3′, H-4′), 5.94 (d, J = 6.7 Hz, 1H, H-1), 4.89 (d, J = 6.7 Hz, 1H, OH) ppm. ^{13}C NMR (101 MHz, DMSO-d_6): δ 153.5, 141.3, 110.2, 107.2, 79.4 ppm.

*8-Chloro-2-(furan-2-yl)-3H-imidazo[4,5-c]quinoline and Tautomer (**20**).* Chloroquinolinediamine **24** (290.9 mg, 1.50 mmol, 1.0 equiv) and metabisulfite adduct **25** (301.8 mg, 1.51 mmol, 1.0 equiv) were suspended in 4.5 mL of DMF and heated to 100 °C under reflux cooling for 4.5 h. The mixture was cooled to ambient temperature and poured onto a small amount of chipped ice. The resulting voluminous precipitate was collected by filtration, washed with water, and dried in vacuo to yield **20** (387.0 mg, 96%) as a light-brown solid. An analytical sample was purified by semipreparative RP HPLC (H_2O/ACN 95:5 → 50:50). ^1H NMR (400 MHz, DMSO-d_6): δ 14.12 (s, 0.6H, NH), 13.90 (s, 0.4H, NH*), 9.23 (s, 0.6H, H-5), 9.16 (s, 0.4H, H-5*), 8.60 (d, J = 2.3 Hz, 0.6H, H-10), 8.40 (d, J = 1.9 Hz, 0.4H, H-10*), 8.13 (d, J = 9.0 Hz, 1H, H-7), 8.06 (s, 1H, H-5′), 7.70 (dd, J = 2.4, 8.9 Hz, 1H, H-8), 7.33 (d, J = 3.1 Hz, 0.4H, H-3'*), 7.40 (d, J = 3.3 Hz, 0.6H, H-3′), 6.81 (dd, J = 1.8, 3.5 Hz, 1H, H-4′) ppm. ^{13}C NMR (101 MHz, DMSO-d_6): δ 145.6 (C-2), 145.3 (C-5′), 144.9 (C-2′), 144.7 (C-5), 142.0 (C-6a), 138.1 (C-5*), 137.8 (C-4), 133.8 (C-10b), 131.8 (C-7), 131.7 (C-7*), 130.7 (C-9), 127.6 (C-8), 127.4 (C-8*), 121.0 (C-10), 120.3 (C-10*), 118.1 (C-10a), 112.7 (C-4′), 112.2 (C-3'*), 111.4 (C-3′) ppm. HRMS (ESI): m/z calcd for $C_{14}H_8N_3OCl$ $[M + H]^+$: 270.0434, found: 270.0440.

*tert-Butyl-8-Chloro-2-(furan-2-yl)-3H-imidazo[4,5-c]quinoline-3-carboxylate (**27**).* Imidazoquinoline **20** (151.1 mg, 560 μmol, 1.0 equiv) was suspended in 30 mL of dry THF under an atmosphere of nitrogen. Subsequently, di-*tert*-butyldicarbonate (Boc_2O, 239.0 mg, 1.10 mmol, 2.0 eq) and DMAP (7.9 mg, 65 μmol, 0.1 equiv) were added to the reaction mix, followed by heating to reflux (72 °C) until TLC showed complete conversion. After cooling to ambient temperature, the reaction was stopped by the addition of 30 mL of H_2O. The brown solution was transferred to a separating funnel and extracted with ethyl acetate (total volume: 200 mL). The combined organic phase was dried over Na_2SO_4 and evaporated under reduced pressure. The resulting brown residue was taken up in 3 mL of DCM and purified by flash chromatography (SiO_2, DCM/MeOH 0.5 → 4%) to yield **27** (164.0 mg, 79%) as a dark-brown solid. ^1H NMR (400 MHz, DMSO-d_6): δ 9.45 (s, 1H, H-5), 8.43 (dd, J = 0.3, 2.4 Hz, 1H, H-10), 8.19 (d, J = 9.0 Hz, 1H, H-7), 8.10 (dd, J = 0.8, 1.8 Hz, 1H, H-5′), 7.81 (dd, J = 2.5, 9.0 Hz, 1H, H-8), 7.37 (dd, J = 0.8, 3.5 Hz, 1H, H-3′), 6.80 (dd, J = 1.8, 3.5 Hz, 1H, H-4′), 1.62 (s, 9H, H-4″) ppm. ^{133}C NMR (101 MHz, DMSO-d_6): δ 146.8 (C-1″), 146.1 (C-5′), 145.1 (C-2), 143.1 (C-2′), 143.0 (C-6a), 142.3 (C-10b), 139.4 (C-5), 132.1 (C-9), 131.6 (C-7), 129.0 (C-8), 127.1 (C-4), 121.8 (C-10a), 120.6 (C-10), 116.1 (C-3′), 112.1 (C-4′), 87.3 (C-3″), 27.3 (3x C-4″) ppm. HRMS (ESI): m/z calcd for $C_{19}H_{16}N_3O_3Cl$ $[M + H]^+$: 370.0958, found: 370.0965.

*3-(tert-Butoxycarbonyl)-8-Chloro-2-(furan-2-yl)-3H-imidazo[4,5-c]quinoline-5-oxide (**28**).* Imidazo-quinoline carboxylate **27** (82.5 mg, 223 μmol, 1.0 equiv) was weighed in a heat-dried microwave vessel and dissolved in 2 mL of DCM. Then, *meta*-chloroperbenzoic acid (mCPBA, ≤77%, 58.0 mg, 336 μmol, 1.5 equiv) was added, and the reaction mixture was stirred at ambient temperature for 3 h. The clear orange mother liquor was collected with an injection syringe and directly purified by flash chromatography (SiO_2, DCM/MeOH 0 → 10%) to yield **28** (64.0 mg, 74%) as a dark-brown, glassy solid. ^1H NMR (400 MHz, DMSO-d_6): δ 8.98 (s, 1H, H-5), 8.62 (d, J = 9.3 Hz, 1H, H-7), 8.43 (d, J = 2.3 Hz, 1H, H-10), 8.07 (dd, J = 0.8, 1.8 Hz, 1H, H-5′), 7.87 (dd, J = 2.3, 9.3 Hz, 1H, H-8), 7.31 (dd, J = 0.8, 3.5 Hz, 1H, H-3′), 6.79 (dd, J = 1.8, 3.5 Hz, 1H, H-4′), 1.58 (s, 9H, H-4″) ppm. ^{13}C NMR (101 MHz, DMSO-d_6): δ 146.5 (C-1″), 146.0 (C-5′), 144.8 (C-2), 143.0 (C-2′), 137.5 (C-6a), 134.7 (C-9), 133.8 (C-10b), 129.7 (C-8), 127.4 (C-4), 126.0 (C-5), 122.6 (C-7), 122.4 (C-10a), 121.4 (C-10), 115.7 (C-3′), 112.1 (C-4′), 87.6 (C-3″), 27.2 (C-4″) ppm. LC−MS (ESI): m/z = 386.1 (100%, ^{35}Cl) $[M + H]^+$, 388.1 (37%, ^{37}Cl) $[M + H]^+$.

*C,H-Functionalization by Conversion of N-Oxide **28** (**19**, **32**).* The Boc-protected imidazoquinoline-5-oxide **28** (62.0 mg, 161 μmol, 1.0 equiv) was solved in 2 mL of a mixture of dry DCM and benzotrifluoride (1:1) under an atmosphere of argon. The clear yellow solution was injected into a heat-dried, argon-filled microwave vessel through its septum cap. The reaction mixture was cooled down to 0 °C, followed by the addition of a solution of *p*-toluenesulfonyl chloride (TsCl, 48.4 mg, 254 μmol, 1.6 equiv) in 1 mL of dry DCM. The reaction was stirred for 4 h, during which a colorless precipitate began to form. Subsequently, ammonia (7M in MeOH, 290 μL, 2 mmol, 12.4 equiv) was added to the mixture before the ice bath was removed. The reaction was stirred for 3 h at ambient temperature before an additional volume of 290 μL of ammonia was added, followed by stirring overnight (16 h). The mother liquor was filtered, and the filtrate was charged with 1 g of silica, followed by the evaporation of the solvents. The resulting residue was purified twice by flash chromatography (SiO_2, 1.: DCM/MeOH/NH_4OH_{conc} (0.1 Vol %), 0.5 → 7.0% MeOH, 2.: DCM/MeOH 0.5 → 4.0%), yielding **32** as a faintly yellow solid (22 mg, 45%). The filter cake of the mother liquor was washed thoroughly with DCM and dried under reduced pressure. The crude residue was taken up in 50 mL of ethyl acetate. The solution was washed three times with saturated sodium bicarbonate solution and once with brine. The combined organic phases were dried over sodium sulfate and filtrated. The filtrate was charged with 1 g of silica and evaporated under reduced pressure. The residue was purified by flash chromatography [SiO_2, DCM/MeOH/NH_4OH_{conc} (0.1 Vol %), 0.5 → 7.0% MeOH], yielding **19** as a tan solid (9 mg, 20%).

*8-Chloro-2-(furan-2-yl)-3H-imidazo[4,5-c]quinolin-4-Amine and Tautomer (**19**).* Yield: 9 mg (20%) ^1H NMR (400 MHz, DMSO-d_6): δ = 13.77 (s, 0.74H, NH), 13.19 (s, 0.26H, NH*), 8.24 (s, 1H, H-10), 7.99 (s, 1H, H-5′), 7.57 (d, J = 8.9 Hz, 1H, H-7), 7.42 (dd, J = 2.4, 8.9 Hz, 1H, H-8), 7.19 (s, 1H, H-3′), 6.88 (s, 2H, NH2), 6.79 (dd, J = 1.5, 3.0 Hz, 1H, H-4′) ppm. ^{13}C NMR (101 MHz, DMSO-d_6): δ = 152.0 (C-5), 147.4 (C-2), 145.3 (C-2′), 144.6 (C-5′), 143.0 (C-6a), 133.4 (C-10b), 128.1 (C-4), 127.2 (C-7), 127.0 (C-8), 124.9 (C-9), 120.4 (C-10), 115.5 (C-10a), 112.5 (C-4′), 110.0 (C-3′) ppm. HRMS (ESI): m/z calcd for $C_{14}H_9N_4OCl$ $[M + H]^+$: 285.0543, found: 285.0546.

*4,8-Dichloro-2-(furan-2-yl)-3H-imidazo[4,5-c]quinoline and Tautomer (**32**).* Yield: 22 mg (45%) ^1H NMR (400 MHz, DMSO-d_6): δ = 14.39 (s, 0.85H, NH), 14.22 (s, 0.15H, NH*), 8.59 (d, J = 2.1 Hz, 0.86H, H-10), 8.39 (s, 0.14H, H-10*), 8.08 (d, J = 1.4 Hz, 1H, H-5′), 8.05 (d, J = 9.0 Hz, 1H, H-7), 7.74 (dd, J = 2.4, 8.9 Hz, 1H, H-8), 7.52 (s, 0.15H, H-3'*), 7.37 (d, J = 3.3 Hz, 0.85H, H-3′), 6.82 (dd, J = 1.7, 3.4 Hz, 1H, H-4′) ppm. ^{133}C NMR (101 MHz, DMSO-d_6): δ = 145.6 (C-5′), 144.4 (C-2′, C-5), 142.4 (C-2), 141.2 (C-6a), 135.5 (C-10b), 134.7 (C-4), 131.2 (C-9), 130.7 (C-7), 128.5 (C-8), 121.2 (C-10), 117.9 (C-10a), 112.8 (C-4′), 112.1 (C-3′) ppm. HRMS (ESI): m/z calcd for $C_{14}H_7N_3OCl_2$ $[M + H]^+$: 304.0040, found: 304.0044.

Phenotypic BMP Activator Screening Assay. The assay was previously described by us in detail.[4] Briefly, clear-bottom 384-well plates (Greiner) were coated with 0.1% gelatine and 500 cells (CGR8-mESC-*Myh6*-GFP)/well were seeded using a Multidrop microplate dispenser (Thermo Scientific) in an LIF-free medium to allow spontaneous differentiation (day 0). After 3 days, compounds and DMSO were added to the wells in quadruplicates for 1° screening (triplicates for IC_{50} determinations) with an Echo Liquid Handler (Labcyte). To stimulate cardiac differentiation, DMH-1 (0.5 μM) was added in a reduced serum-containing medium (6% FBS) and rh-BMP-4 (10 ng/mL) was added as a control manually to monitor rescue effects. After treatment for 24 h, the medium was changed to

complete the LIF-free mESC medium and refreshed on days 7 and 9. On day 11, cells were fixed with 4% PFA and stained with DAPI (1:1000 of 1 mg/mL stock in PBS) for 20 min at room temperature. Cells were washed (PBS) on a Microplate washer ELx405 (BioTek), sealed with adhesive aluminum foil (nerbe plus, Winsen, Germany), and centrifuged at 500 rpm for 1 min, and plates were imaged on an Image Xpress MicroXL System (Molecular Devices) connected to an automated microplate mover Orbitor RS. GFP levels and DAPI count were quantified with MetaXpress Software 6 using a multi-wavelength scoring algorithm and analyzed by "Mean Stain Integrated Intensity" and "Total Cells". Data are shown as mean ± standard error of the mean (SEM) of *Myh6*-GFP levels normalized to the DMH-1 induction level or cell count for DAPI levels. IC_{50} values were calculated with GraphPad Prism 5 or Quattro Workflow 3.1. Cell count levels below 70% of DMH-1 were considered false-positive due to cytotoxicity.

Zebrafish Assays. *RNA Synthesis and in Situ Hybridization.* Templates for antisense DIG RNA probes were generated by cutting plasmid DNA with suitable restriction enzymes at the 5′ end of the cDNA, followed by a single step of phenol/chloroform extraction and precipitation of the linearized vector with 2.5 volume of EtOH and a final concentration of 0.3 M NaOAc. DIG RNA probes were generated with suitable RNA polymerase depending on the orientation of the insert and vector type using a DIG labeling mix (Roche). Embryos for in situ hybridization were collected between 50 and 80% epiboly stage. In situ hybridization with digoxygenin-incorporated antisense RNA probes was done as decribed.[56] Fish embryo raising and staging were as described.[18]

Embryo Treatments. For treatments, several batches of 15−20 fertilized eggs were selected and transferred into wells of a 24-well plate. Embryos were treated with DMSO (control) and different concentrations of **1a** compound at 3 hpf stage until 50 to 80% epiboly stage for in situ hybridization assays or until 24 hpf stage for the analysis of their phenotypes. All embryos were grown in an incubator at 28 °C.

Murine Osteoblast Differentiation Assay.[4] C2C12 cells were seeded at a density of 2000 cells/well in DMEM, supplemented with 6% heat-inactivated FBS, GlutaMAX, and penicillin−streptomycin in 384-well plates (Greiner). Cells were grown for 16 h, and compounds/DMSO were added in triplicates with the Echo Liquid Handler (Labcyte). For osteogenic induction, BMP-4 was added to the wells (7.5 ng/mL) after compound addition and cells were incubated for 72 h. ALP activity was determined with pre-mixed substrate-containing CDP-Star in the lysis buffer (1:100), and luminescence was measured on a Paradigm Reader after 1 h. For analysis, the ALP activity of 7.5 ng/mL BMP-4 in DMSO was set to 100% to calculate synergistic activity of tested compounds. Cell toxicity was analyzed for selected compounds after compound treatment (72 h) using the CellTiterGlo assay (Promega).

Human Osteoblast Mineralization Assay.[4] Human SaOS-2 cells were cultured in DMEM (DMEM/F12, Sigma), supplemented with 10% FCS and 1% penicillin−streptomycin. To induce osteogenic differentiation, the medium was supplemented with 10 mM ß-glycerophosphate, 0.2 mM ascorbic acid, and 10 nM dexamethasone. Cells were seeded in 96-well plates (8×10^3 cells/well), and DMSO/compound 2 ng/mL BMP-4 or BMP-2, was added. DMSO (0.01%) was used as a vehicle control, and cells were incubated for 11 days. Afterward, the cell culture medium was carefully aspirated and the cells were washed with PBS (w/o Ca^{2+}, Mg^{2+}). After aspiration of PBS, the cells were fixed with neutral-buffered formalin (4%) for 30 min at room temperature and then washed three times with aqua dest. 100 μL of the Alizarin Red S solution [2 g of Alizarin Red S (Sigma) in 100 mL of aqua dest., pH 4.1−4.3] was added into the wells for 20 min. After aspiration of the staining solution, the cells were washed four times with aqua dest. For quantification of mineralization, 100 μL of a 10% cetylpyridium chloride solution (dissolved in aqua dest.) was added to each well and incubated for 20 min at room temperature. 100 μL was loaded in duplicate to a 96-well plate and measured at 562 nm (Tecan, Infinite F200 Pro multiplate reader).

Luciferase Reporter Gene Assays. Reporter gene assays were performed in HEK293T cells as described in detail before.[4] Briefly, cells were transiently transfected in batch with a luciferase reporter gene containing plasmid with Lipofectamine 2000 (Invitrogen) and replated after 14 h on 96-well plates (2.5×10^4 cells/well) in 1% FBS-containing DMEM for 2 h, followed by addition of test compounds, DMSO, and the respective growth factor (10 ng/mL) in triplicates. Cells were lyzed after 22 h, and luciferase activity was measured on a Paradigm Reader (Molecular Devices) using a Dual Luciferase Assay Kit (Promega) or ONE-Glo Reagent (Promega). In addition, compounds were tested for non-specific luciferase modulation using a 293/Luc cell line, containing a stably expressing firefly luciferase gene. To determine sonic hedgehog activity, stably transfected NIH3T3 cells with a firefly-GLI-responsive promoter were used and hedgehog signaling was induced by purmorphamine (3 μM) for 48 h before readout.

Quantitative Real-Time PCR. In general, RNA was isolated from differentiating mESCs or C2C12 at indicated time points after treatment. Osteogenic expression marker profiles were obtained from compound-treated (compounds, DMSO, and BMP-4) C2C12 cells by plating 1×10^5 cells/well in 24-well plates after growth in the differentiation medium for indicated times. Cells were washed and lysed, and RNA was isolated with an RNeasy Mini Kit (Qiagen) according to the manufacturer's protocol. cDNA was synthesized using a qScript cDNA Synthesis Kit (Quanta Bioscience) on a PCR thermocycler, and RT-qPCR was performed with a Takyon SYBR Master Mix (Eurogentec) on a Lightcycler 480 (Roche). Primers were purchased from IDT (Integrated DNA Technologies, Leuven), and all sequences are listed in the Supporting Information (Table S1). For determination of the relative gene expression, the ΔΔCp method was used. All data points are shown as mean of triplicates ± standard deviation (SD), normalized to DMSO unless stated otherwise.

PCR Array Analysis. After 24 h treatments, C2C12 were washed and lysed, and RNA was isolated with the RNeasy Mini Kit (Qiagen). The cDNA was synthesized using an RT^2 First Strand Kit (Qiagen) on a PCR thermocycler according to the manufacturer's protocol. The array was performed using an RT^2 SYBR Green qPCR Mastermix (Qiagen) on an RT^2 Profiler PCR Array (PAMM-035ZG) for the mouse TGFβ/BMP signaling pathway.

Western Blot Analysis. Immunoblots were generated as described in detail before.[4] In brief, C2C12 cells were grown and treated in 100 mm dishes. After treatment, cells were collected and subcellular fractionation was performed to separate nuclear and cytosolic protein fractions. Protein content was determined using a Pierce BCA Protein Assay Kit (Thermo Scientific). The samples were separated on polyacrylamide gels containing 0.5% trichloroethanol to measure total protein per lane after UV illumination. Signals from specific antibody staining were normalized to total protein per lane, and quantification and analysis were performed with LabImage 1D software.

Cell Painting Assay. The described assay was performed using U2OS cells, closely following the method described by the Carpenter group (2016).[33] A detailed protocol for the staining and imaging procedure can be found in the Supporting Information. The generated images were processed with the *Cell Profiler* package (version 3.0.0) on a computing cluster of the Max Planck Society to extract 1716 cell features per microscope site.[33] The data were then further aggregated as medians per well (9 sites → 1 well) and then over the three replicates. Further analysis was performed with custom *Python* (https://www.python.org/) scripts using the Pandas (https://pandas.pydata.org/) and Dask (https://dask.org/) data processing libraries as well as the *Scientific Python* (https://scipy.org/) package. From the total set of 1716 features, a subset of 579 highly reproducible and robust features was determined using a described procedure,[57] which can also be found in the Supporting Information. The phenotypic compound profile is then determined as the list of z-scores of all features for one compound. In addition to the phenotypic profile, an induction value was determined for each compound as the fraction of significantly changed features, in percent. Similarities of phenotypic profiles were calculated from the correlation distances

between two profiles (similarity = 1 − correlation distance), and the compounds with the most similar profiles were determined from a set of 3000 reference compounds that was also measured in the assay.[58]

Full-Length CK1-Kinase Assay. Expression and purification of 6xHis-CK1δ (transcription variant 1; NM_001893), 6xHis-CK1ε (transcription variant 1; NM_152221), and 6xHis-CK1α (transcription variant 3; NM_001271741) were performed as described elsewhere.[59] For the initial screening and IC_{50} determination, in vitro kinase reactions were performed in triplicates at 30 °C in a total reaction volume of 15 μL containing 10 mM $MgCl_2$, 100 μM EDTA, 10 μM ATP, 2.5 μM α-casein (substrate), kinase (500 nM 6xHis-CK1δ or 6xHis-CK1ε; 50 nM 6xHis-CK1α), 10 μM to 5 nM compound, and 0.4 pmol [γ-^{32}P]-ATP in 25 mM Tris−HCl (pH 7.0). Reactions were stopped after 30 min by adding 3 μL of 5 × SDS loading buffer and boiling at 95 °C for 5 min. Proteins in the reaction mix were separated by SDS-PAGE and stained with Coomassie Brilliant Blue R250 (Waldeck GmbH & Co. KG, Muenster, Germany). Radioactively labeled proteins were visualized by autoradiography. Phosphorylated proteins were excised from dried gels, and phosphate incorporation was quantified via Cherenkov counting. Phosphate incorporation was normalized to the solvent control (DMSO).

Michaelis−Menten Kinetics. Determination of V_{max} (maximal reaction velocity) and $K_{m(ATP)}$ (concentration of ATP, at which half of V_{max} is achieved) was performed as described elsewhere.[59] For Michaelis−Menten kinetics, in vitro kinase reactions were performed as described above with various ATP concentrations in a range from 0.5 to 100 μM ATP in the presence of an inhibitor at a concentration of the determined IC_{50} or IC_{25} or DMSO as a vehicle control. Reaction samples were processed as described above. Reaction velocity (V) was plotted over ATP concentration and fitted to the Michaelis−Menten model using GraphPad Prism 7 (GraphPad Software, La Jolla, CA, USA). In order to determine the type of inhibition, linearization according to Lineweaver−Burk was performed by double reciprocal illustration of substrate concentration and velocity.

Molecular Modeling. The software package Maestro DrugDiscoverySuite (Maestro Version 12.6.144, MMshare Version 5.2.144, Release 2020−4, Platform Windows-x64), Schrödinger LLC (New York, USA), was used for molecular modeling studies. The protein structure 3R7R of the RCSB protein data bank (PDB) was used as a PI3Kα receptor model; 5DXT was used as a PI3Kα receptor model. The protein structure was prepared with the Protein Preparation Wizard. Bond orders were adjusted, hydrogen atoms were added, disulfide bonds were optimized, water molecules within a distance of >5 Å to heteroatoms were deleted, and H-bonding within the protein structure was optimized using the standard protocol in Glide. The geometry of the protein was improved in a simplified, restricted optimization using OPLS3e force field. In the process, heavy atoms within an RMSD of 0.3 Å were converged. Receptor grids were created using the tool Glide. The geometry of **1a** (CGS-15943) was optimized using LigPrep. Binding modes were calculated with the tool Glide using the Standard Precision (SP) mode.

Crystallography. For structural studies, a C-terminally truncated version of CK1δ (1−294, tCK1δ) was produced as described previously.[60] In brief, tCK1δ, His_6-tagged tCK1δ was recombinantly expressed in BL21 (DE3) TaKaRa 2 *Escherichia coli* cells (Clontech) and afterward purified by immobilized metal affinity chromatography. For co-crystallization of tCK1δ with **1a** (CGS-15943), protein stock solution (10 mg·mL^{-1}) was mixed 30:1 with 10 mM of **1a** (solubilized in DMSO) and incubated for 30 min at room temperature. Sitting drop crystallization trials were set up at room temperature with drop ratios of 150 nL protein/inhibitor solution to 150 nL precipitant solution. Crystals appeared after 3 to 7 days in drops containing 0.2 M sodium malonate (pH = 5.0), 20% (*w*/*v*) PEG 3350. For data collection, these crystals were cryo-protected by swiping them through the reservoir solution supplemented with 15% (*v*/*v*) Polyethylenglykol 400 and subsequently flash-frozen. Diffraction data were collected at beamline P13 at the PETRA/EMBL Hamburg, German Synchrotron Research Centre (*DESY*) campus, Hamburg, Germany. Details on X-ray data collection and refinement statistics can be found in the Supporting Information (Table S3).

Statistical Analysis. Statistical analysis between two groups was performed with an unpaired *t*-test and a set confidence level of 95% of three replicates and $n \geq 3$ independent biological experiments unless stated otherwise. Symbols for the significance level are indicated as follows, unless stated otherwise: ns, not significant; *$p < 0.05$; **$p < 0.01$; ***$p < 0.001$. IC_{50} and EC_{50} values were calculated with GraphPad Prism 5−7.

■ ASSOCIATED CONTENT

Accession Codes

The co-crystal structure of **1a** (CGS-15943)-bound CK1δ has been deposited under PDB ID7NZY.

■ AUTHOR INFORMATION

Corresponding Author

Dennis Schade − *Department of Pharmaceutical and Medicinal Chemistry, Institute of Pharmacy, Christian-Albrechts University of Kiel, 24118 Kiel, Germany; Partner Site Kiel, DZHK, German Center for Cardiovascular Research, 24105 Kiel, Germany;* orcid.org/0000-0002-5515-1821; Phone: (+49) 431 880 1176; Email: schade@pharmazie.uni-kiel.de; Fax: (+49) 431 880 1352

Authors

Fabian Wesseler − *Faculty of Chemistry and Chemical Biology, Technical University Dortmund, 44227 Dortmund, Germany; Department of Pharmaceutical and Medicinal Chemistry, Institute of Pharmacy, Christian-Albrechts University of Kiel, 24118 Kiel, Germany; Compound Management and Screening Center COMAS, Max Planck Institute of Molecular Physiology (MPI), 44227 Dortmund, Germany*

Stefan Lohmann − *Department of Pharmaceutical and Medicinal Chemistry, Institute of Pharmacy, Christian-Albrechts University of Kiel, 24118 Kiel, Germany*

Daniel Riege − *Department of Pharmaceutical and Medicinal Chemistry, Institute of Pharmacy, Christian-Albrechts University of Kiel, 24118 Kiel, Germany*

Jonas Halver − *Faculty of Chemistry and Chemical Biology, Technical University Dortmund, 44227 Dortmund, Germany*

Aileen Roth − *Department of General and Visceral Surgery, University Hospital Ulm, 89081 Ulm, Germany*

Christian Pichlo − *Department of Chemistry, University of Cologne, 50939 Cologne, Germany*
Sabrina Weber − *Institute of Biological and Chemical Systems - Biological Information Processing at Karlsruhe Institute of Technology (KIT), 76344 Eggenstein-Leopoldshafen, Germany*
Masanari Takamiya − *Institute of Biological and Chemical Systems - Biological Information Processing at Karlsruhe Institute of Technology (KIT), 76344 Eggenstein-Leopoldshafen, Germany*
Eva Müller − *Department of Orthopedic Surgery, Otto-von-Guericke University, 39120 Magdeburg, Germany*
Jana Ketzel − *Department of Pharmaceutical and Medicinal Chemistry, Institute of Pharmacy, Christian-Albrechts University of Kiel, 24118 Kiel, Germany*
Jana Flegel − *Faculty of Chemistry and Chemical Biology, Technical University Dortmund, 44227 Dortmund, Germany*
Adrian Gihring − *Department of General and Visceral Surgery, University Hospital Ulm, 89081 Ulm, Germany*
Sepand Rastegar − *Institute of Biological and Chemical Systems - Biological Information Processing at Karlsruhe Institute of Technology (KIT), 76344 Eggenstein-Leopoldshafen, Germany*
Jessica Bertrand − *Department of Orthopedic Surgery, Otto-von-Guericke University, 39120 Magdeburg, Germany*
Ulrich Baumann − *Department of Chemistry, University of Cologne, 50939 Cologne, Germany*
Uwe Knippschild − *Department of General and Visceral Surgery, University Hospital Ulm, 89081 Ulm, Germany*
Christian Peifer − *Department of Pharmaceutical and Medicinal Chemistry, Institute of Pharmacy, Christian-Albrechts University of Kiel, 24118 Kiel, Germany;* orcid.org/0000-0003-1532-7826
Sonja Sievers − *Compound Management and Screening Center COMAS, Max Planck Institute of Molecular Physiology (MPI), 44227 Dortmund, Germany; Max-Planck-Institute of Molecular Physiology, 44227 Dortmund, Germany*
Herbert Waldmann − *Faculty of Chemistry and Chemical Biology, Technical University Dortmund, 44227 Dortmund, Germany; Max-Planck-Institute of Molecular Physiology, 44227 Dortmund, Germany;* orcid.org/0000-0002-9606-7247

Author Contributions

D.S. conceived and designed the project. F.W., D.R., J.H., A.R., C.P., S.W., M.T., E.M., J.F., S.R., and J.B. performed the biological and biochemical experiments. S.L. and J.K. performed the chemical syntheses. All the authors analyzed and critically discussed the results. F.W., S.L., D.R., and D.S. prepared the manuscript.

Notes

The authors declare no competing financial interest.

■ ACKNOWLEDGMENTS

We thank the Dortmund Protein Chemistry Facility for providing high-quality LIF and Christiane Pfaff and Carina Birke for excellent technical assistance at the COMAS screening facility. Melissa Zietz, Petra Köster, Meike Wichmann, Sven Wichmann, and Elena Brunstein are gratefully acknowledged for excellent technical assistance. We also would like to thank Ulrich Girreser for his excellent service and support with the spectroscopic characterization of synthesized compounds. Michael Schulz is acknowledged for his help with the FACS instrument. This work was in part supported by funds from the German Federal Ministry of Science and Education (BMBF, grant 131605).

■ ABBREVIATIONS

ActA, activin A; AhR, aryl hydrocarbon receptor; ALK, activin receptor-like kinase; ALP, alkaline phosphatase; ATP, adenosine triphosphate; BMP, bone morphogenetic protein; BRE, BMP-responsive element; cDNA, complementary DNA; CHK-1, checkpoint kinase 1; CK1, casein kinase 1; CPA, Cell Painting Assay; DMH-1, dorsomorphin-homolog 1; DNA-PK, DNA-dependent protein kinase; ESC, embryonic stem cell; Eve1, even-skipped-like 1; FBS, fetal bovine serum; GF, growth factor; GSC, goosecoid; GSK3, glycogen synthase kinase 3; Hpf, hours post fertilization; Id, inhibitor of DNA binding; LIF, leukemia inhibitory factor; Luc, luciferase; mESC, murine embryonic stem cell; Myh6, myosin heavy chain 6; Ocn, osteocalcin; Osx, osterix; PD, PD407824; PDD, phenotypic drug discovery; PI3K, phosphoino-sitol-3 kinase; Pm, Purmorphamine; RGA, reporter gene assay; RNA, ribonucleic acid; Runx2, Runt-related transcription factor 2 (CBF-α-1); SBE, SMAD-binding element; SD, standard deviation; SEM, standard error of mean; TCF, T-cell factor; TDD, target-centric drug discovery; TGFβ, transforming growth factor-β.

■ REFERENCES

(1) Tian, S. S.; Lamb, P.; King, A. G.; Miller, S. G.; Kessler, L.; Luengo, J. I.; Averill, L.; Johnson, R. K.; Gleason, J. G.; Pelus, L. M.; Dillon, S. B.; Rosen, J. A Small, Nonpeptidyl Mimic of Granulocyte-colony-stimulating Factor. *Science* **1998**, *281*, 257−259.
(2) Duffy, K. J.; Erickson-miller, C. L. The Discovery of Eltrombopag, An Orally Bioavailable TpoR Agonist. In *Target Validation in Drug Discovery*; Metcalf, B. W., Dillon, S., Eds.; Academic Press, 2007, pp 241−254.
(3) Beck, H.; Jeske, M.; Thede, K.; Stoll, F.; Flamme, I.; Akbaba, M.; Ergüden, J. K.; Karig, G.; Keldenich, J.; Oehme, F.; Militzer, H. C.; Hartung, I. V.; Thuss, U. Discovery of Molidustat (BAY 85-3934): A Small-Molecule Oral HIF-Prolyl Hydroxylase (HIF-PH) Inhibitor for the Treatment of Renal Anemia. *ChemMedChem* **2018**, *13*, 988−1003.
(4) Wesseler, F.; Riege, D.; Puthanveedu, M.; Halver, J.; Müller, E.; Bertrand, J.; Antonchick, A. P.; Sievers, S.; Waldmann, H.; Schade, D. Probing Embryonic Development Enables the Discovery of Unique Small-Molecule Bone Morphogenetic Protein Potentiators. *J. Med. Chem.* **2022**, *65*, 3978−3990.
(5) Salazar, V. S.; Gamer, L. W.; Rosen, V. BMP Signalling in Skeletal Development, Disease and Repair. *Nature Rev. Endocrinol.* **2016**, *12*, 203−221.
(6) Wagner, D. O.; Sieber, C.; Bhushan, R.; Börgermann, J. H.; Graf, D.; Knaus, P. BMPs: From Bone to Body Morphogenetic Proteins. *Sci. Signal.* **2010**, *3*, mr1.
(7) Lowery, J. W.; Rosen, V. Bone Morphogenetic Protein-Based Therapeutic Approaches. *Cold Spring Harb. Perspect. Biol.* **2018**, *10*, a022327.
(8) Genthe, J. R.; Min, J.; Farmer, D. M.; Shelat, A. A.; Grenet, J. A.; Lin, W.; Finkelstein, D.; Vrijens, K.; Chen, T.; Guy, R. K.; Clements, W. K.; Roussel, M. F. Ventromorphins: A New Class of Small Molecule Activators of the Canonical BMP Signaling Pathway. *ACS Chem. Biol.* **2017**, *12*, 2436−2447.
(9) Feng, L.; Cook, B.; Tsai, S.-Y.; Zhou, T.; LaFlamme, B.; Evans, T.; Chen, S. Discovery of a Small-Molecule BMP Sensitizer for Human Embryonic Stem Cell Differentiation. *Cell Rep* **2016**, *15*, 2063−2075.

(10) Cook, B.; Walker, N.; Zhang, Q.; Chen, S.; Evans, T. The Small molecule DIPQUO Promotes Osteogenic Differentiation via Inhibition of Glycogen Synthase Kinase 3-beta Signaling. *J. Biol. Chem.* **2021**, *296*, 100696.
(11) Larraufie, M. H.; Gao, X.; Xia, X.; Devine, P. J.; Kallen, J.; Liu, D.; Michaud, G.; Harsch, A.; Savage, N.; Ding, J.; Tan, K.; Mihalic, M.; Roggo, S.; Canham, S. M.; Bushell, S. M.; Krastel, P.; Gao, J.; Izaac, A.; Altinoglu, E.; Lustenberger, P.; Salcius, M.; Harbinski, F.; Williams, E. T.; Zeng, L.; Loureiro, J.; Cong, F.; Fryer, C. J.; Klickstein, L.; Tallarico, J. A.; Jain, R. K.; Rothman, D. M.; Wang, S. Phenotypic Screen Identifies Calcineurin-Sparing FK506 Analogs as BMP Potentiators for Treatment of Acute Kidney Injury. *Cell Chem. Biol.* **2021**, *28*, 1271−1282.
(12) Zinski, J.; Tajer, B.; Mullins, M. C. TGF-beta Family Signaling in Early Vertebrate Development. *Cold Spring Harb. Perspect. Biol.* **2018**, *10*, a033274.
(13) Hata, A.; Seoane, J.; Lagna, G.; Montalvo, E.; Hemmati-Brivanlou, A.; Massagué, J. OAZ uses Distinct DNA- and Protein-Binding Zinc Fingers in Separate BMP-Smad and Olf Signaling Pathways. *Cell* **2000**, *100*, 229−240.
(14) Rastegar, S.; Friedle, H.; Frommer, G.; Knöchel, W. Transcriptional Regulation of Xvent Homeobox Genes. *Mech. Dev.* **1999**, *81*, 139−149.
(15) Cai, W.; Albini, S.; Wei, K.; Willems, E.; Guzzo, R. M.; Tsuda, M.; Giordani, L.; Spiering, S.; Kurian, L.; Yeo, G. W.; Puri, P. L.; Mercola, M. Coordinate Nodal and BMP Inhibition Directs Baf60c-Dependent Cardiomyocyte Commitment. *Genes Dev.* **2013**, *27*, 2332−2344.
(16) Cunningham, T. J.; Yu, M. S.; McKeithan, W. L.; Spiering, S.; Carrette, F.; Huang, C. T.; Bushway, P. J.; Tierney, M.; Albini, S.; Giacca, M.; Mano, M.; Puri, P. L.; Sacco, A.; Ruiz-Lozano, P.; Riou, J. F.; Umbhauer, M.; Duester, G.; Mercola, M.; Colas, A. R. Id Genes are Essential for Early Heart Formation. *Genes Dev.* **2017**, *31*, 1325−1338.
(17) Svenda, J.; Sheremet, M.; Kremer, L.; Maier, L.; Bauer, J. O.; Strohmann, C.; Ziegler, S.; Kumar, K.; Waldmann, H. Biology-oriented Synthesis of a Withanolide-Inspired Compound Collection Reveals Novel Modulators of Hedgehog Signaling. *Angew. Chem., Int. Ed.* **2015**, *54*, 5596−5602.
(18) Westerfield, M. *The Zebrafish Book. A Guide for the Laboratory Use of Zebrafish (Danio rerio)*; University of Oregon Press: Eugene, 1995; Vol. 3.
(19) Nohe, A.; Keating, E.; Knaus, P.; Petersen, N. O. Signal Transduction of Bone Morphogenetic Protein Receptors. *Cell Signal* **2004**, *16*, 291−299.
(20) Heldin, C. H.; Miyazono, K.; ten Dijke, P. TGF-beta Signalling from Cell Membrane to Nucleus through SMAD proteins. *Nature* **1997**, *390*, 465−471.
(21) Hollnagel, A.; Oehlmann, V.; Heymer, J.; Rüther, U.; Nordheim, A. Id Genes are Direct Targets of Bone Morphogenetic Protein Induction in Embryonic Stem Cells. *J. Biol. Chem.* **1999**, *274*, 19838−19845.
(22) Balo, C.; López, C.; Brea, J. M.; Fernánde, F.; Caamaño, O. Synthesis and Evaluation of Adenosine Antagonist Activity of a Series of [1,2,4]Triazolo[1,5-*c*]quinazolines. *Chem. Pharm. Bull.* **2007**, *55*, 372−375.
(23) Gatta, F.; Del Giudice, M. R.; Borioni, A. Synthesis of [1,2,4]Triazoloquinazoline and [1,2,4]-Triazolo-1,4-benzodiazepine Derivatives. *J. Heterocyclic Chem* **1993**, *30*, 11−16.
(24) Francis, J. E.; Cash, W. D.; Psychoyos, S.; Ghai, G.; Wenk, P.; Friedmann, R. C.; Atkins, C.; Warren, V.; Furness, P.; Hyun, J. L.; et al. Structure-Activity Profile of a Series of Novel Triazoloquinazoline Adenosine Antagonists. *J. Med. Chem.* **1988**, *31*, 1014−1020.
(25) Gelotte, K. O.; Mason, D. N.; Meckler, H.; Shieh, W.-C.; Starkey, C. M. An Efficient Synthesis of the Novel Triazoloquinazoline Adenosine Antagonist, CGS 15943. *J. Heterocyclic Chem.* **1990**, *27*, 1549−1552.
(26) Van Galen, P. J.; Nissen, P.; Van Wijngaarden, I.; Ijzerman, I. J.; Soudijn, W. 1*H*-Imidazo[4,5-*c*]quinolin-4-amines: Novel Non-xanthine Adenosine Antagonists. *J. Med. Chem.* **1991**, *34*, 1202−1206.
(27) Gerster, J. F.; Lindstrom, K. J.; Miller, R. L.; Tomai, M. A.; Birmachu, W.; Bomersine, S. N.; Gibson, S. J.; Imbertson, L. M.; Jacobson, J. R.; Knafla, R. T.; Maye, P. V.; Nikolaides, N.; Oneyemi, F. Y.; Parkhurst, G. J.; Pecore, S. E.; Reiter, M. J.; Scribner, L. S.; Testerman, T. L.; Thompson, N. J.; Wagner, T. L.; Weeks, C. E.; Andre, J. D.; Lagain, D.; Bastard, Y.; Lupu, M. Synthesis and Structure-activity-relationships of 1*H*-Imidazo[4,5-*c*]quinolines that Induce Interferon Production. *J. Med. Chem.* **2005**, *48*, 3481−3491.
(28) Williams, M.; Francis, J.; Ghai, G.; Braunwalder, A.; Psychoyos, S.; Stone, G. A.; Cash, W. D. Biochemical Characterization of the Triazoloquinazoline, CGS 15943, a Novel, Non-xanthine Adenosine Antagonist. *J. Pharmacol. Exp. Ther.* **1987**, *241*, 415−20.
(29) Ghai, G.; Francis, J. E.; Williams, M.; Dotson, R. A.; Hopkins, M. F.; Cote, D. T.; Goodman, F. R.; Zimmerman, M. B. Pharmacological Characterization of CGS 15943A: a Novel Non-xanthine Adenosine Antagonist. *J. Pharmacol. Exp. Ther.* **1987**, *242*, 784−90.
(30) Köse, M.; Gollos, S.; Karcz, T.; Fiene, A.; Heisig, F.; Behrenswerth, A.; Kieć-Kononowicz, K.; Namasivayam, V.; Müller, C. E. Fluorescent-Labeled Selective Adenosine A2B Receptor Antagonist Enables Competition Binding Assay by Flow Cytometry. *J. Med. Chem.* **2018**, *61*, 4301−4316.
(31) O'Donnell, E. F., 3rd; Jang, H. S.; Liefwalker, D. F.; Kerkvliet, N. I.; Kolluri, S. K. Discovery and Mechanistic Characterization of a Select Modulator of AhR-regulated Transcription (SMAhRT) with Anti-cancer Effects. *Apoptosis* **2021**, *26*, 307−322.
(32) Schneidewind, T.; Brause, A.; Pahl, A.; Burhop, A.; Mejuch, T.; Sievers, S.; Waldmann, H.; Ziegler, S. Morphological Profiling Identifies a Common Mode of Action for Small Molecules with Different Targets. *ChemBioChem* **2020**, *21*, 3197−3207.
(33) Bray, M. A.; Singh, S.; Han, H.; Davis, C. T.; Borgeson, B.; Hartland, C.; Kost-Alimova, M.; Gustafsdottir, S. M.; Gibson, C. C.; Carpenter, A. E. Cell Painting, a High-content Image-based Assay for Morphological Profiling using Multiplexed Fluorescent Dyes. *Nat. Protoc.* **2016**, *11*, 1757−1774.
(34) Ziegler, S.; Sievers, S.; Waldmann, H. Morphological Profiling of Small Molecules. *Cell Chem. Biol.* **2021**, *28*, 300−319.
(35) Bosc, N.; Meyer, C.; Bonnet, P. The Use of Novel Selectivity Metrics in Kinase Research. *BMC Bioinformatics* **2017**, *18*, 17.
(36) Bozatzi, P.; Dingwell, K. S.; Wu, K. Z.; Cooper, F.; Cummins, T. D.; Hutchinson, L. D.; Vogt, J.; Wood, N. T.; Macartney, T. J.; Varghese, J.; Gourlay, R.; Campbell, D. G.; Smith, J. C.; Sapkota, G. P. PAWS1 Controls Wnt Signalling through Association with Casein Kinase 1alpha. *EMBO Rep.* **2018**, *19*, No. e44807.
(37) Fallica, B.; Maffei, J. S.; Villa, S.; Makin, G.; Zaman, M. Alteration of Cellular Behavior and Response to PI3K Pathway Inhibition by Culture in 3D Collagen Gels. *PLoS One* **2012**, *7*, No. e48024.
(38) Garces, A. E.; Stocks, M. J. Class 1 PI3K Clinical Candidates and Recent Inhibitor Design Strategies: A Medicinal Chemistry Perspective. *J. Med. Chem.* **2019**, *62*, 4815−4850.
(39) Fok, J. H. L.; Ramos-Montoya, A.; Vazquez-Chantada, M.; Wijnhoven, P. W. G.; Follia, V.; James, N.; Farrington, P. M.; Karmokar, A.; Willis, S. E.; Cairns, J.; Nikkilä, J.; Beattie, D.; Lamont, G. M.; Finlay, M. R. V.; Wilson, J.; Smith, A.; O'Connor, L. O.; Ling, S.; Fawell, S. E.; O'Connor, M. J.; Hollingsworth, S. J.; Dean, E.; Goldberg, F. W.; Davies, B. R.; Cadogan, E. B. AZD7648 is a Potent and Selective DNA-PK Inhibitor that Enhances Radiation, Chemotherapy and Olaparib Activity. *Nat. Commun.* **2019**, *10*, 5065.
(40) Pomel, V.; Klicic, J.; Covini, D.; Church, D. D.; Shaw, J. P.; Roulin, K.; Burgat-Charvillon, F.; Valognes, D.; Camps, M.; Chabert, C.; Gillieron, C.; Françon, B.; Perrin, D.; Leroy, D.; Gretener, D.; Nichols, A.; Vitte, P. A.; Carboni, S.; Rommel, C.; Schwarz, M. K.; Rückle, T. Furan-2-ylmethylene Thiazolidinediones as Novel, Potent, and Selective Inhibitors of Phosphoinositide 3-kinase Gamma. *J. Med. Chem.* **2006**, *49*, 3857−3871.

(41) Viñals, F.; López-Rovira, T.; Rosa, J. L.; Ventura, F. Inhibition of PI3K/p70 S6K and p38 MAPK Cascades Increases Osteoblastic Differentiation Induced by BMP-2. *FEBS Lett.* **2002**, *510*, 99−104.
(42) Gámez, B.; Rodríguez-Carballo, E.; Graupera, M.; Rosa, J. L.; Ventura, F. Class I PI-3-Kinase Signaling Is Critical for Bone Formation Through Regulation of SMAD1 Activity in Osteoblasts. *J. Bone Miner. Res.* **2016**, *31*, 1617−1630.
(43) Kang, H.; Chang, W.; Hurley, M.; Vignery, A.; Wu, D. Important Roles of PI3Kgamma in Osteoclastogenesis and Bone Homeostasis. *Proc. Natl. Acad. Sci. U.S.A.* **2010**, *107*, 12901−12906.
(44) Janovská, P.; Normant, E.; Miskin, H.; Bryja, V. Targeting Casein Kinase 1 (CK1) in Hematological Cancers. *Int. J. Mol. Sci.* **2020**, *21*, 9026.
(45) Rodríguez-Carballo, E.; Ulsamer, A.; Susperregui, A. R.; Manzanares-Céspedes, C.; Sánchez-García, E.; Bartrons, R.; Rosa, J. L.; Ventura, F. Conserved Regulatory Motifs in Osteogenic Gene Promoters Integrate Cooperative Effects of Canonical Wnt and BMP pathways. *J. Bone Miner. Res.* **2011**, *26*, 718−729.
(46) Beurel, E.; Grieco, S. F.; Jope, R. S. Glycogen synthase kinase-3 (GSK3): Regulation, Actions, and Diseases. *Pharmacol. Ther.* **2015**, *148*, 114−131.
(47) Sato, N.; Meijer, L.; Skaltsounis, L.; Greengard, P.; Brivanlou, A. H. Maintenance of Pluripotency in Human and Mouse Embryonic Stem Cells through Activation of Wnt Signaling by a Pharmacological GSK-3-specific Inhibitor. *Nat. Med.* **2004**, *10*, 55−63.
(48) Waddell, D. S.; Liberati, N. T.; Guo, X.; Frederick, J. P.; Wang, X. F. Casein Kinase Iepsilon Plays a Functional Role in the Transforming Growth Factor-beta Signaling Pathway. *J. Biol. Chem.* **2004**, *279*, 29236−29246.
(49) Vincent, F.; Nueda, A.; Lee, J.; Schenone, M.; Prunotto, M.; Mercola, M. Phenotypic Drug Discovery: Recent Successes, Lessons Learned and New Directions. *Nature Rev. Drug Discov.* **2022**, 1.
(50) Vincent, F.; Loria, P. M.; Weston, A. D.; Steppan, C. M.; Doyonnas, R.; Wang, Y. M.; Rockwell, K. L.; Peakman, M. C. Hit Triage and Validation in Phenotypic Screening: Considerations and Strategies. *Cell Chem. Biol.* **2020**, *27*, 1332−1346.
(51) Knust, H.; Achermann, G.; Ballard, T.; Buettelmann, B.; Gasser, R.; Fischer, H.; Hernandez, M. C.; Knoflach, F.; Koblet, A.; Stadler, H.; Thomas, A. W.; Trube, G.; Waldmeier, P. The Discovery and Unique Pharmacological Profile of RO4938581 and RO4882224 as Potent and Selective GABAA alpha5 Inverse Agonists for the Treatment of Cognitive Dysfunction. *Bioorg. Med. Chem. Lett.* **2009**, *19*, 5940−5944.
(52) Yoo, E.; Salunke, D. B.; Sil, D.; Guo, X.; Salyer, A. C.; Hermanson, A. R.; Kumar, M.; Malladi, S. S.; Balakrishna, R.; Thompson, W. H.; Tanji, H.; Ohto, U.; Shimizu, T.; David, S. A. Determinants of Activity at Human Toll-like Receptors 7 and 8: Quantitative Structure-activity Relationship (QSAR) of Diverse Heterocyclic Scaffolds. *J. Med. Chem.* **2014**, *57*, 7955−7970.
(53) Kim, Y. C.; Ji, X. D.; Jacobson, K. A. Derivatives of the Triazoloquinazoline Adenosine Antagonist (CGS15943) are Selective for the Human A3 Receptor Subtype. *J. Med. Chem.* **1996**, *39*, 4142−4148.
(54) Takada, S.; Sasatani, T.; Chomei, N.; Adachi, M.; Fujishita, T.; Eigyo, M.; Murata, S.; Kawasaki, K.; Matsushita, A. Synthesis and Structure-activity Relationships of Fused Imidazopyridines: a new Series of Benzodiazepine Receptor Ligands. *J. Med. Chem.* **1996**, *39*, 2844−2851.
(55) Abdullaziz, M. A.; Abdel-Mohsen, H. T.; El Kerdawy, A. M.; Ragab, F. A. F.; Ali, M. M.; Abu-bakr, S. M.; Girgis, A. S.; El Diwani, H. I. Design, Synthesis, Molecular Docking and Cytotoxic Evaluation of Novel 2-Furylbenzimidazoles as VEGFR-2 inhibitors. *Eur. J. Med. Chem.* **2017**, *136*, 315−329.
(56) Oxtoby, E.; Jowett, T. Cloning of the Zebrafish Krox-20 gene (krx-20) and its Expression during Hindbrain Development. *Nucleic Acids Res.* **1993**, *21*, 1087−1095.
(57) Woehrmann, M. H.; Bray, W. M.; Durbin, J. K.; Nisam, S. C.; Michael, A. K.; Glassey, E.; Stuart, J. M.; Lokey, R. S. Large-scale Cytological Profiling for Functional Analysis of Bioactive Compounds. *Mol. Biosyst.* **2013**, *9*, 2604−2617.
(58) Grigalunas, M.; Burhop, A.; Zinken, S.; Pahl, A.; Gally, J. M.; Wild, N.; Mantel, Y.; Sievers, S.; Foley, D. J.; Scheel, R.; Strohmann, C.; Antonchick, A. P.; Waldmann, H. Natural Product Fragment Combination to Performance-diverse Pseudo-natural Products. *Nat. Commun.* **2021**, *12*, 1883.
(59) Roth, A.; Gihring, A.; Göser, F.; Peifer, C.; Knippschild, U.; Bischof, J. Assessing the Inhibitory Potential of Kinase Inhibitors In Vitro: Major Pitfalls and Suggestions for Improving Comparability of Data Using CK1 Inhibitors as an Example. *Molecules* **2021**, *26*, 4898.
(60) Halekotte, J.; Witt, L.; Ianes, C.; Krüger, M.; Bührmann, M.; Rauh, D.; Pichlo, C.; Brunstein, E.; Luxenburger, A.; Baumann, U.; Knippschild, U.; Bischof, J.; Peifer, C. Optimized 4,5-Diarylimidazoles as Potent/Selective Inhibitors of Protein Kinase CK1delta and Their Structural Relation to p38alpha MAPK. *Molecules* **2017**, *22*, 522.